Universität Stuttgart

Geodätisches Institut

The role of multispectral image transformations in change detection

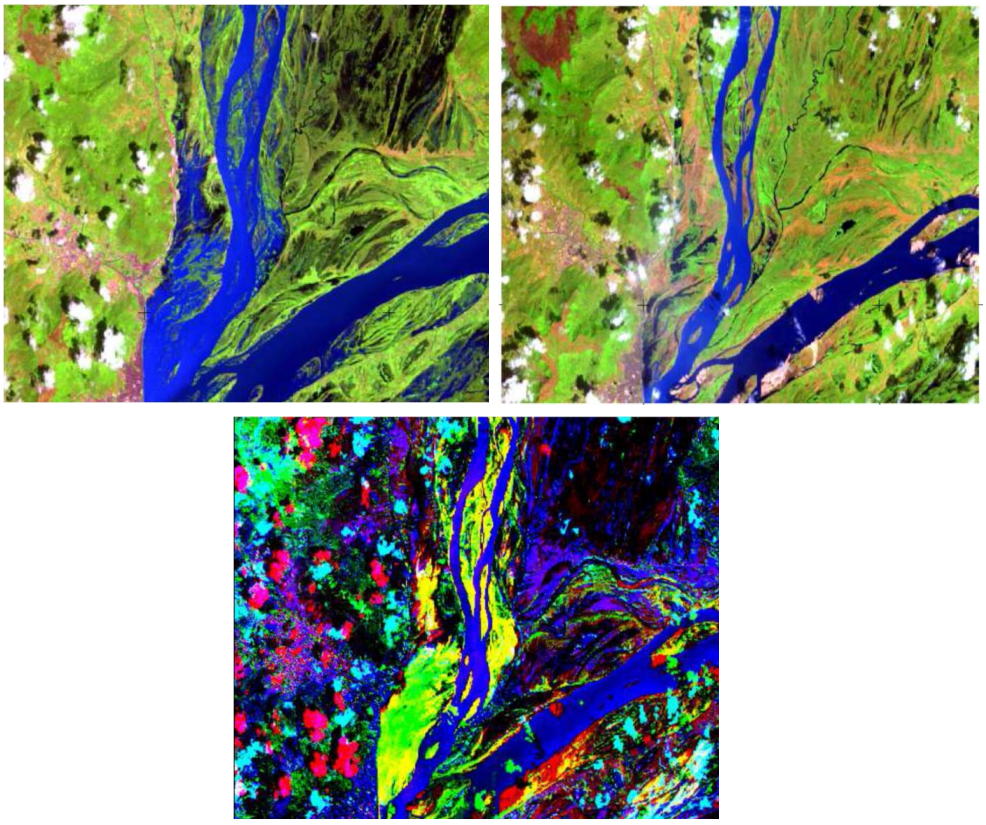

Omid Elmi

Master Thesis

Stuttgart, January 2015

Supervisor: Prof. Dr.-Ing. Nico Sneeuw
Universität Stuttgart

Erklärung der Urheberschaft

Ich erkläre hiermit an Eides statt, dass ich die vorliegende Arbeit ohne Hilfe Dritter und ohne Benutzung anderer als der angegebenen Hilfsmittel angefertigt habe; die aus fremden Quellen direkt oder indirekt übernommenen Gedanken sind als solche kenntlich gemacht. Die Arbeit wurde bisher in gleicher oder ähnlicher Form in keiner anderen Prüfungsbehörde vorgelegt und auch noch nicht veröffentlicht.

Ort, Datum Unterschrift

Abstarct

In recent decades, remote sensing techniques have been applied as a powerful tool to provide temporal variation of Earth related phenomena. To understand the impact of climate change and human activities on Earth water resources, monitoring the variation of water storage over a long period is a primary issue. On the other hand, this variation is fundamental to estimate the hydroelectric power generation variation and fresh water recreation. Among the spaceborne sensors, optical and SAR satellite imagery provide the opportunity to monitor the spatial change in coastline, which can serve as a way to determine the water extent repeatedly in an appropriate time interval.

While water absorbs nearly all the sunlight in near-infrared wavelength, the water bodies appear very dark at this band in an optical image. So applying a threshold on the image histogram is a common way to build the water mask. Despite its straightforward procedure, precise distinctions among water bodies may not be possible in some regions or seasons because of the complicated relationship between water and land and also because of the effect of vegetation.

As well as thresholding, other change detection method are widely used to monitor the extent of water bodies. Multispectral transformation analyses like PCA and CCA are able to highlight the important information about the change in all spectral bands and also to reduce the dimension of data. In this way, their potential to improve the quality of satellite images and also reduce the noise level must be assessed.

In this thesis, we have two general objectives. First improving the quality of the multispectral image applying PCA on spectral bands and then reconstructing the image using just a certain number of PCs. Number of the PCs and the selecting strategy appropriate PCs are the main challenge of this procedure. Highlighting the change between two multispectral images applying transformation like PCA and CCA is the other objective. Interpreting the transformed images are not straightforward and in most cases, comparing with the original images could be a solution. We examine different scenarios to examine the performance of the spectral transformations in change detection.

Contents

List of Figures

List of Tables

List of abbreviations

ANN	Artificial Neural Networks
AVHRR	Advanced Very High Resolution Radiometer
CCA	Canonical Correlation Analysis
DTM	Digital Terrain Model
Envisat	Environmental Satellite
EM	Expectation Maximization
EOF	Empirical Orthogonal Function
ERS	European Remote Sensing satellite
ESA	European Space Agency
GIS	Geospatial Information Systems
GRACE	Gravity Recovery And Climate Experiment
KT	Kauth Thomas transformation
MAD	Multivariate Alteration Detection
MAF	Maximum Autocorrelation Factor
MSS	Multispectral Scanner
MODIS	Moderate Resolution Imaging Spectroradiometer
NASA	National Aeronautics and Space Administration
NIR	Near Infrared
NDVI	Normalized Difference Vegetation Index
OLI	Operational Land Imager
PCA	Principal Component Analysis
SAR	Synthetic aperture radar
SRTM	Shuttle Radar Topography Mission
SVD	Singular Value Decomposition

SWIR Short-Wave Infrared

TIRS Thermal Infrared Sensor

Chapter 1

Introduction

1.1 Introduction to water cycle monitoring

Inland surface water bodies cover only a small fraction of the Earth surface but they have a great effect on sustaining life on Earth and they play a primary role in the global water cycle and climate change (Prigent et al., 2007). Lakes and reservoirs are highly valuable for their freshwater supply (Alsdorf et al., 2007). Lakes constitute important habitats and food resources for a diverse array of fish, aquatic life, and wildlife. Lake ecosystems can undergo rapid environmental changes, often leading to significant declines in their natural functions. Exposed to external effects from the atmosphere, their watersheds and groundwater, lakes are subject to change through time. In urban areas their condition is highly fragile because they are vulnerable for pollution. Rivers are also classified as inland surface water. They have been essential not only to humans, but to all life on earth, ever since life began. Plants and animals grow and congregate around rivers simply because water is so essential to all life. Cities are typically built and developed around rivers. For humans, rivers are diverted for flood control, irrigation, power generation, municipal uses and even waste disposal.

Despite their importance to human life, our knowledge about spatial and temporal variation of river discharge and total water storage of lakes is surprisingly poor, because our understanding is based on in situ measurements. Given insufficient monitoring from in situ gauge networks, and without any outlook of improvement, spaceborne approaches have been investigated (Sneeuw et al., 2014). In the last two decades, remote sensing techniques have proven their ability to measure different hydrological parameters. They are summarized in Alsdorf et al. (2007) as follows:

- **Water area:** water area or inundation area can be measured using different satellite optic images like Landsat or Moderate Resolution Imaging Spectroradiometer (MODIS) (Tourian et al., 2015) and SAR images like European Remote Sensing Satellite (ERS) or Enviromental Satellite (Envisat) (Papa et al., 2008; Smith and Pavelsky, 2009). Despite their partial success, they suffer from poor spatial resolution, cloud coverage in optical images or the effect of the wind in SAR images.

- **Water level:** Satellite altimetry missions have successful history for a few decades to measure the ocean surface elevation and also the level of inland water bodies. Also its capability to estimate river discharge in big rivers have been evaluated (Alsdorf and Lettenmaier, 2003; Crétaux and Birkett, 2006; Tourian et al., 2013). Apart from the relatively poor temporal resolution (35 days for Envisat and 10 days for TOPEX/Poseidon), a large number of inland water bodies remain unmeasured because of the pointwise data sampling of satellite altimetry missions.
- **Total water storage:** Apart from geometric parameters, change in total water storage as a physical variable is observed by Gravity Recovery And Climate Experiment (GRACE) (Sneeuw et al., 2014). The change in the amount of different forms of water (surface, subsurface, ice and atmosphere) leads to change in the Earth gravity which is measured by GRACE. A lot of effort to reduce the noise and to improve the spatial and temporal resolution of GRACE are done but still GRACE-related products are rarely satisfactory. GRACE is also unable to distinguish between surface and subsurface water which is also an important drawback of it in hydrological studies.
- **Other parameters:** More than mentioned parameters measured directly, some parameters are derived from them. For example, water slope can be calculated employing water level and a digital terrain model (DTM) like shuttle radar topography mission (SRTM) (Birkett et al., 2002). Romeiser et al. (2007) introduced a novel method to measure stream velocity based on interferometric SAR technique. Tarpanelli et al. (2013) assessed a relationship between river discharge and ratio between water and land pixel values in the optical images.

Establishing a coherent observational basis of these quantities from space allow us to refine global water cycle models by improving our knowledge about interseasonal and interannual variations in surface water storage volumes as well as their impact on precipitation, evaporation, infiltration and runoff.

Optical and SAR satellite imagery missions provide the opportunity to monitor the spatial change in coastline, which can serve as a way to determine the water extent repeatedly in an appropriate time interval. In recent decades, the monitoring of Earth related phenomena is more feasible than before because a lot of images from different missions are available. Recent missions provide images with better spatial and temporal resolution, so comprehensive interpretation about hydrological objects is expected.

In the Figure (1.1), different optic and SAR missions are presented. The advanced very high resolution radiometer (AVHRR) with approximately 1×1 km pixel size has been available since 1980 and widely applied for water body and wetland monitoring (Papa et al., 2006). Different Landsat missions continue gathering images in various multispectral bands from the Earth since 1980. Recently Landsat 8 with 30 m spatial resolution provides images monthly. The use of daily snapshots of MODIS with 250 m

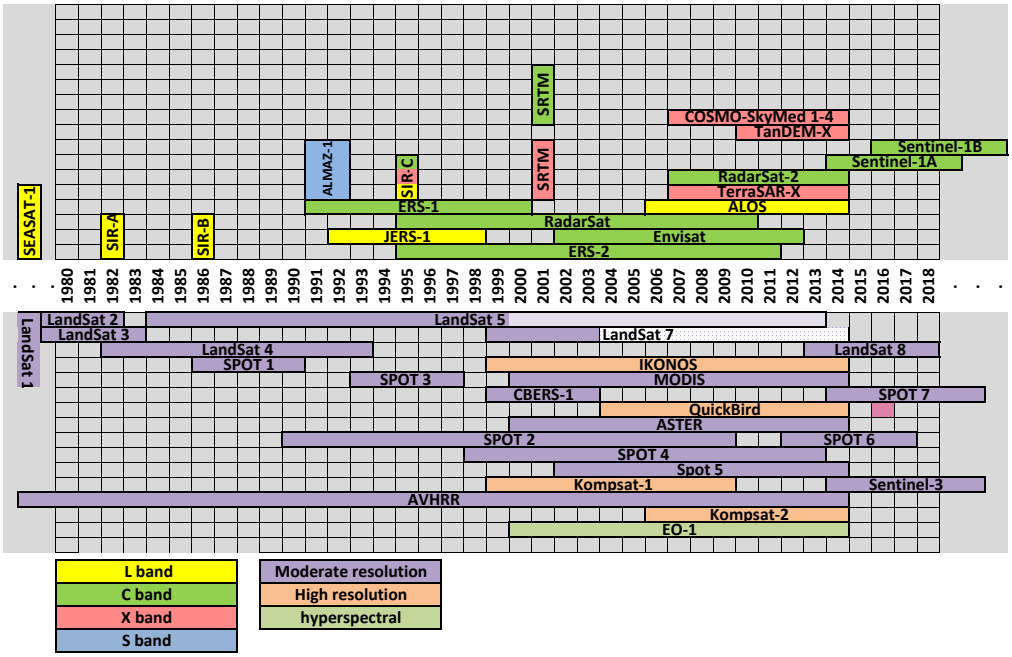

Figure 1.1: Different optic and SAR missions

resolution are also very common in monitoring the Earth phenomena. In the future, Sentinel-2 will provide images with better resolution (10 m, 20 m, 60 m) and also high revisit time (5 days). For the SAR missions, images from ERS-1, ERS-2 and Envisat in C band are the main sources for water area monitoring spatially in the tropical area which is rainy most of the year (Smith et al., 1996). TerraSAR-X in X band provides high resolution images with 1, 2 and 3 meter pixel size every 2 days. Martinis et al. (2009) used TerraSAR-X images to develop a method to detect the flood. In 2014, Sentinel-1A as the most advanced SAR satellite system as launched to expand our understanding about the Earth characteristics.

1.2 Introduction to change detection

Change detection is the process of identifying differences in the state of an object or phenomenon by observing it at different times (Singh, 1989). Timely and accurate change detection of Earth's surface features help us to understand better the relationship and interaction between human and natural phenomena (Lu et al., 2004). Lu et al. (2004) categorized different change detection applications using remote sensing technologies in ten aspects, e.g. land-use and land-cover change, forest and vegetation change, wetland change, landscape change and urban change. Considering the importance of monitoring the change in Earth surface features and also different aspects, many change detection methods have been developed and new techniques are constantly developed. Lu et al. (2004) summarized change detection methods into

seven groups.

- **Algebra**: Most of the techniques in this category determine the changed areas by selecting a threshold. Image differencing, image regression and image rationing are some examples of this group. Finding the suitable threshold to identify the changed areas is the difficulty of these methods.
- **Transformation**: These methods establish a numerical relationship between different bands of one image or different bands of different images to emphasize the change in the transformed components. Principal component analysis (PCA), the Tasselled Cap transformation and multivariate alteration detection (MAD) transformations are applied in Munyati (2004); Bustos et al. (2011); Nielsen (2007*a*, 2011). These methods also need thresholds to highlight the change area and, in some cases, interpretation of transformed images is difficult.
- **Classification**: The methods in this group apply different image classification techniques in the multitemporal images to monitor the change. For example in the post-classification comparison method, all images are classified separately after which a pixel by pixel comparison is implemented to detect the change. Spectral-temporal combined analysis, expectation maximization(EM) change detection and artificial neural networks (ANN) are some examples in this category.
- **GIS**: Integration of geospatial information systems (GIS) and remote sensing methods to detect the change in the image is the main advantage of this category. Most of the GIS based change detection applications are focused on urban areas because GIS tools are very powerful to deal with multi-source data processing.
- **Advanced models**: In these methods, a linear or non-linear model is applied to the images. They are converted to physically based parameters or pixel fractions. For example, a spectral mixture model was applied to detect the change of land-cover in Amazon (Adams et al., 1993).
- **Visual analysis**: In this category, change in shape, size and pattern of the subject area in the multi-temporal images is detected by visual interpretation of a well experienced analyst. This method was widely used in the past, because the capability of computers to handle large amount of data was poor.

Selecting an efficient change detection technique among the large amount of different methods is a fundamental step to reach acceptable results. This decision must be based on the knowledge about the application and available in situ and remote sensing data. In other words, the first step in a change detection application is studying carefully the application and the data and to find the best method to apply to them.

While water absorbs nearly all the sunlight in the near infrared wavelength, water bodies appear very dark at this domain in an optical image. In a SAR image, water bodies also appear dark because the smooth surface of water acts like a mirror for the incident radar pulse and most of the energy is reflected away according to the law of specular

reflection. As a result, very little energy is scattered back to the radar sensor. Unlike the clear difference between water and land, precise distinction between wetlands, rivers and lakes may not be possible in some regions or seasons. Identifying and characterizing wetlands globally is further complicated by their distribution throughout tropical to boreal environments encompassing a wide variety of vegetation cover, hydrological regime, natural seasonality, and land-use impacts (Prigent et al., 2007).

Applying a threshold to backscattering values to binarize images is the most straightforward method in change detection and pattern recognition algorithms (Li and Lee, 1993). In remote sensing, this method is common because of its efficiency and easy implementation. Thresholding is also widely used in inland water body monitoring to develop a water mask. Under ideal conditions, most of the water body extent can be detected correctly by this method but various sources of error and the complex relationship between water and land in coastal areas necessitate researchers to define the threshold value in a supervised manner using visual inspection of the image histogram or manual trial-and-error procedures (Townsend, 2001; Brivio et al., 2002; Cao, 2013) or automatic thresholding procedures (Bazi et al., 2007).

As well as thresholding, other change detection methods are widely used to detect the change in water body extents. For example, images differences (Joyce et al., 2009) and image ratios (Martinis et al., 2013) are commonly applied to determine water bodies. Unsupervised classification methods like k-means clustering also applied (Gao et al., 2012). The method is an effective tool to delineate water extent in each snapshot. PCA as a method of change detection for an inland wetland is presented in Munyati (2004). Supervised classification methods like maximum likelihood are applied to establish a binary decision classifier on SAR and optic images in (Wang, 2004). Klein et al. (2014) take advantage of a static water mask and a DTM to restrict the search area and improve the accuracy of water extent determination.

The ability to highlight important information of all spectral bands of an image and also to reduce the dimension of data, multispectral transformation analyses are widely applied in remote sensing applications. Switzer and Green (1984) introduced maximum autocorrelation factor analysis. Gong (1993) applied PCA on the difference of two images acquired at different times to emphasize the change in primary principal components. In (Nielsen et al., 2002), EOF was applied to sea surface temperature analysis. MAD and MAF analysis and the combined MAD/MAF transformation based on CCA were introduced in (Nielsen et al., 1998). As they presented in their paper, this transformation is insensitive to differences in gain settings in measuring device, or to linear radiometric and atmospheric coastal spheric correction schemes. Canty and Nielsen (2008) applied iteratively re-weighted MAD transformation for radiometric normalization of multitemporal images. More sophisticated methods in this category are listed in Nielsen (2011).

1.3 Objective of this thesis

In this thesis, the potential of a number of spectral transformations to improve the change detection procedure is evaluated. Here, monitoring the change in the water bodies over time is our main focus. Our main objectives are summarized:

- Enhance the quality of an image by reducing the noise level and then compare the enhanced images to define the change more easily and precisely. PCA is an appropriate tool for this goal and selecting the right PC to reconstruct the image is the main concern.

- Emphasize and highlight the spatial change between two multitemporal images applying different transformation. MAD transformation has a great ability to highlight the change between two data set and also MAF transformation magnifies the area in which the correlation with the neighbouring pixel is high. Also, PCA has the ability to highlight the change between two multitemporal data if they merged together. This process can specify not only pixels which have noticeable difference from the mean pixels value but also the area whose pixel values have changed over time.

1.4 Case study and data

The study area for this study is the Niger river. The inland delta of the Niger river is one of the most fragile ecosystems of Sub-Saharan Africa. Patterns of land cover and land use vary extremely due to pre-flood and post-flood hydrological conditions of Niger river and its tributaries. The Niger River is the third largest river (4200 km) in Africa, and the fourteenth longest river in the world. The river flows through Guinea, Mali, Niger, Benin, Nigeria and it discharges on the Gulf of Guinea. The Niger Basin is composed of very diverse ecoregions ranging from the arid Sahel to the extremely wet coastal Niger Delta. (McGinley, 2013). The confluence of two river ,Niger and Bani, is located in this delta and they provide approximately 1490 m^3/s water for the delta. The amount of precipitation in the basin is highly variable between dry and wet season. Therefore, the area of river changes with very complex patterns depending on the topography of the river channels or the presence of vegetation, and on the total amount of water filling the rivers. During flood periods, the land is also subject to noticeable vegetation growth, mixed with water and dry soil. So, reliable frequent observation of the water extent, spatial distribution and temporal variation of the river's floodplain is vital.

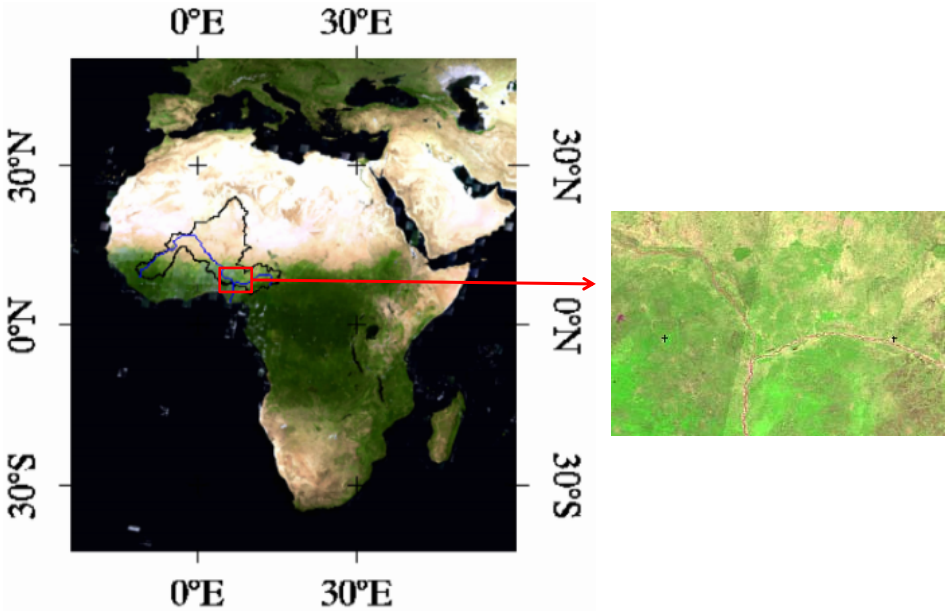

Figure 1.2: An image of Niger basin and Niger river

1.4.1 MODIS

In this thesis, we will mainly use MODIS images. MODIS is a scientific instrument launched by NASA. Terra satellite was launched in 1999 and the aqua part joined it in 2002. Both of them have been active till now and provide images on daily basis globally. It provides high radiometric sensitive (12 bit) image in 36 spectral bands from 0.405 ¯m to 14.3385 ¯m. MODIS acquires data at three different spatial resolutions (2 bands in 250 m, 5 bands in 500 m and 29 bands in 1 km). This wide variety of spectral and spatial options and also daily data acquisitions make MODIS an important source for land surface boundaries and properties, atmospheric water vapour and temperature, surface temperature, ocean color.

Many standard MODIS data products are derived from the original data for different purposes. For example, level one data (MOD01) is useful for calibration. Some products are widely applied in atmosphere studies (for example MOD07, MOD04, MOD06), and for land monitoring applications (MOD16, MOD011 and MOD09).

In this thesis, the MODIS surface reflectance product (MOD09) is used. This product is an estimate of the surface spectral reflectance for each band as it would have been measured at ground level if there were no atmospheric scattering or absorption. Seven different spectral bands with 500 m spatial resolution are available in this product. Malfunctioning of one of the detectors in the Terra MODIS causes sharp and repetitive noise in band 5 image, so this band is omitted and here we have just six different bands.

Table 1.1: List of available bands in MODIS MOD09

Band	spectral range [nm]	Description
1	620–670	red
2	841–876	NIR
3	459–479	blue
4	545–565	green
5	1230–1250	SWIR 1
6	1628–1652	SWIR 2
7	2105–2155	SWIR 3

Table 1.2: List of available bands in Landsat 7

Band	Spectral range [nm]	Description
1	450–520	blue-green
2	520–610	green
3	630–690	red
4	760–900	reflected IR
5	1550–1750	reflected IR
6	1040–1250	thermal
7	2080–2350	reflected IR
8	520–900	panchromatic

1.4.2 Landsat

In two parts of this thesis, images from Landsat 7 and Landsat 8 are also used. The first Landsat satellite acquired images from the Earth surface in 1972. Since then, the Landsat project continuously provide worldwide images in different spectral bands. These remote sensing images are a valuable resource for agriculture, geology, forestry, mapping and global change researches.

Landsat 7 was launched in 1999. Its orbit is sun-synchronous and the satellite orbits the Earth at 705 km altitude. The satellite revisit a certain area every 16 days in an ideal situation. Landsat 7 carries the enhanced thematic mapper plus (ETM+), providing 6 different spectral bands in visible and infrared domain with 30 m spatial resolution, a thermal band with 60 m and a 15 m panchromatic band.
Landsat 8 was launched in 2013 and until now it is the most advanced optical imagery system available. Its orbit and revisit time is more or less like Landsat 7. Landsat 8 carries two push broom sensors: the operational land imager (OLI) and thermal infrared sensor (TIRS), both of which provide improved signal to noise ratio and 12 bit radiometric quantization of the data. The OLI provides data in 8 different spectral bands with 30 m resolution and one panchromatic band with 15 m spatial resolution. TIRS captures data in two long wave thermal bands with 100 m resolution.

Table 1.3: List of available bands in Landsat 8

Band	Spectral range [nm]	Description
1	430–450	coastal-aerosol
2	450–510	blue
3	530–590	green
4	640–670	red
5	850–880	NIR
6	1570–1650	SWIR 1
7	2110–2290	SWIR 2
8	500–680	panchromatic
9	1360–1380	cirrus
10	1060–1119	TIRS 1
11	1150–1251	TIRS 2

1.5 Structure of this thesis

In this thesis, each of the determined objectives will be investigated in the following chapters. In chapter two, the mathematical aspects of PCA, MAD and MAF transformations are discussed. Reducing the noise in a multispectral image applying PCA is our main aim in chapter three. To do this, different techniques to retrieve important information about water content form the original image will be investigated. In section four, multispectral transformations are applied as a tool for change detection. We will apply MAD and MAD/MAF on two multitemporal images to investigate their strength in change detection. Then, PCA are applied to a merged data set to highlight the change between them . At the end, there is a brief chapter with conclusions and outlook.

Chapter 2

Multispectral transformations of image data

2.1 Introduction

Spectral transformations generate new sets of image components combining original multispectral image bands. The new components represent an alternative description of the original data while they are related to the old brightness values via a linear operator. The transformed image may make evident features not discernible in the original data or, alternatively, it might be possible to preserve the essential information content of the image with a reduced number of the transformed dimensions (Richards and Jia, 1999). In change detection applications, a key issue is the change mask should not contain unimportant or nuisance forms of change like sensor noise, or atmospheric absorption (Radke et al., 2005). Nielsen (2007*a*) mentions that nontrivial change includes :

- An additive shift in mean level (offset) or a multiplicative shift in calibration of a measuring device (gain).
- Data normalization or calibration schemes that are linear (affine) in the gray values of the original variables.
- Transformations such as principal component (PC) or maximum autocorrelation factor (MAF) transformations can not detect among dataset.

Moreover multispectral transformations can be applied as a tool to enhance the signal to noise ratio level by isolating the noise of remotely sensed images in certain components. Also, a transformed data set may represent a certain physical characteristic of sensed environment.

The multispectral or multidimensional nature of remote sensing image data can be accommodated by constructing a vector space with as many axes or dimensions as there are spectral components associated with each pixel (Richards and Jia, 1999). For example, a Landsat 7 image with 7 spectral bands, can be used to construct a seven-

dimensional vector space.

2.2 Principal component analysis

PCA is a mathematical technique to establish a linear relationship between different values of spectral bands in a way that new components are orthogonal to each other and concentrates the original dataset's variance into the first components.

In remote sensing, PCA has been applied in many cases. Here we summarize it into three groups of application:

- Image compression by considering just a number of primary components instead of all spectral bands;
- Image enhancement by removing some components as the last components are saturated by noise;
- Change detection by highlighting the area in which significant change occurs in the primary components. Examining change in multitemporal data sets by selecting appropriate components.

Suppose that we have a multispectral image with k spectral bands each of which has p rows and q columns. First of all, the images in each band is reshaped as a single column vector of length $(p \times q)$:

$$\mathbf{X} = [x_1, x_2, ..., x_k]. \tag{2.1}$$

Matrix $\mathbf{X}$ is the reshaped form of multispectral image. So, the number of columns is equal to the number of different spectral bands (k) and the number of lines equals $p \times q$. The mean position of the pixels in the spectral space is defined according to

$$m_{\mathrm{x}} = \frac{1}{N} \sum_{n=1}^{N} \mathbf{X}_n, \tag{2.2}$$

where m is the mean pixel value and N is the total number of pixels. To describe the spread of pixels from the mean, the covariance matrix is defined as

$$\Sigma_{\mathrm{x}} = \frac{1}{N-1} \sum_{n=1}^{N} (\mathbf{X}_n - m_{\mathrm{x}})(\mathbf{X}_n - m_{\mathrm{x}})^{\mathrm{T}}. \tag{2.3}$$

If there is any correlation between different pairs of spectral bands, the corresponding off-diagonal element in the covariance matrix is large in comparison to the diagonal elements. On the other hand, the off-diagonal elements are near zero when there is

no correlation among different spectral bands. The aim of principal component transformation is to set new coordinate system in the multispectral space in a way that the covariance matrix in the new coordinate system is diagonal. In other words, in this transformation we are looking for a linear combination of different spectral bands in which transformed data do not correlate. Here, we assume that **W** is the transformed image and **C** is an orthonormal transformation matrix such that the covariance matrix of the transformed image is diagonal and **X** is the original multispectral image

$$\mathbf{W} = \mathbf{C}\,\mathbf{X}. \tag{2.4}$$

In the equation (2.4), **W** and **X** have same dimension ($k \times pq$) and **C** is a $k \times k$ matrix. **W** is

$$\Sigma_{\mathrm{W}} = E\{(\mathbf{W} - m_{\mathrm{W}})(\mathbf{W} - m_{\mathrm{W}})^T\} \tag{2.5}$$

Equations (2.4) and (2.8) can be written as

$$\begin{aligned} m_{\mathrm{W}} &= E(\mathbf{W}) = E(\mathbf{C}\mathbf{X}) = \mathbf{C}m_{\mathrm{x}} && (2.6)\\ \Sigma_{\mathrm{W}} &= E\{(\mathbf{W} - m_{\mathrm{W}})(\mathbf{W} - m_{\mathrm{W}})^T\} \\ &= E\{(\mathbf{C}\mathbf{X} - \mathbf{C}m_{\mathrm{x}})(\mathbf{C}\mathbf{X} - \mathbf{C}m_{\mathrm{x}})^T\} \\ &= \mathbf{C}\,E\{(\mathbf{X} - m_{\mathrm{x}})(\mathbf{X} - m_{\mathrm{x}})^T\}\,\mathbf{C}^T \\ &= \mathbf{C}\,\Sigma_{\mathrm{x}}\,\mathbf{C}^T. && (2.7) \end{aligned}$$

Since Σ_{W} is assumed to be diagonal, the coefficients, **C** can be recognized as the transposed matrix of eigenvectors of Σ_{x}. As a result, Σ_{W} can be identified as the diagonal matrix of eigenvalues of Σ_{x}. The covariance matrix of **W** is

$$\Sigma_{\mathrm{W}} = \begin{bmatrix} \lambda_1 & 0 & & & \\ 0 & \lambda_2 & & & \\ & & \cdot & & \\ & & & \cdot & \\ & & & & \cdot \\ & & & 0 & \lambda_k \end{bmatrix}$$

where k is the number of spectral bands. The elements of the diagonal covariance matrix are the variances of the respective transformed data. The eigenvalues are conventionally arranged in descending order , $\lambda_1 \geq \lambda_2 \geq ... \geq \lambda_k$, so that the largest portion of variance is in W_1, the next maximum variance is in W_2 and so on. To find the eigenvalues and eigenvectors of **X**, to find λs the following equation must be solved:

$$(\mathbf{X} - \lambda I) = 0. \tag{2.8}$$

By knowing the eigenvalues and eigenvectors, now we can calculate the principal components. In general, we can conclude that PC transformation has three major steps. First, calculation of covariance of image data sets. Then, calculation of eigenvalues and eigenvectors and finally, calculation of principal components.

Eklundh and Singh (1993) stated that in remote sensing applications, PCs derived from a covariance matrix do not represent original data well because each band observes sunlight in a different spectrum range, so their origin and scale are varied. To solve this problem, the correlation matrix is used for deriving PCs instead of covariance matrix. In this thesis, we follow their recommendation and use the correlation matrix to derive PCs.

2.2.1 Singular value decomposition

Singular value decomposition (SVD) has some characteristics making it suitable to apply for defining principal components. First, it is a technique to transform correlated variables into a set of uncorrelated ones providing better understanding about the original data. Also it is a method for ordering the data in a way that exhinit the most variation. Finally, by applying SVD, it is possible to find the best approximation for the original data using fewer dimensions (Baker, 2005). SVD is based on a theorem from linear algebra which is any matrix can be broken down into the product of three matrices. Suppose that $\mathbf{A}$ is a matrix with n lines and m columns and $\mathbf{A}$ is not necessary a full rank matrix. We can decompose this matrix into a diagonal and two orthogonal matrices like (2.9)

$$\mathbf{A} = \mathbf{U}\,\Sigma\,\mathbf{V}^T \tag{2.9}$$

where $\mathbf{U}_{n\times n}$ and $\mathbf{V}_{m\times m}$ are two orthogonal matrices and $\Sigma_{n\times m}$ is diagonal. Singular values (σ_i) are diagonal elements of Σ which are non-negative and ordered in a way that $\sigma_1 \geq \sigma_2 \geq ... \geq \sigma_p \geq 0$, where $p = \min(n, m)$. Since $\mathbf{U}$ and $\mathbf{V}$ are orthogonal matrices, their columns form bases for their vector spaces.

Also the singular values of matrix $\mathbf{A}$ solve the following equations.

$$\mathbf{A}\,\mathbf{u} = \sigma\,\mathbf{v} \qquad , \qquad \mathbf{A}^T\,\mathbf{v} = \sigma\,\mathbf{u} \tag{2.10}$$

The vectors $\mathbf{v}$ and $\mathbf{u}$ are known as the right and left singular vectors respectively. The relationship between SVD and eigenvalues are defined through the following equations

$$\mathbf{A}\,\mathbf{A}^T = (\mathbf{U}\,\Sigma\,\mathbf{V}^T)(\mathbf{U}\,\Sigma\,\mathbf{V}^T)^T = \mathbf{U}\,\Sigma\,\mathbf{V}^T\mathbf{V}\,\Sigma\,\mathbf{U}^T = \mathbf{U}\,\Sigma^2\,\mathbf{U}^T \tag{2.11}$$

$$\mathbf{A}^T\,\mathbf{A} = (\mathbf{U}\,\Sigma\,\mathbf{V}^T)^T(\mathbf{U}\,\Sigma\,\mathbf{V}^T) = \mathbf{V}\,\Sigma\,\mathbf{U}^T\mathbf{U}\,\Sigma\,\mathbf{V}^T = \mathbf{V}\,\Sigma^2\,\mathbf{V}^T \tag{2.12}$$

$\mathbf{V}$ and $\mathbf{U}$ can be calculated as the eigenvectors of $\mathbf{A}\ \mathbf{A}^T$ and $\mathbf{A}^T\ \mathbf{A}$ because they are orthogonal so $\mathbf{U}^T = \mathbf{U}^{-1}$ and $\mathbf{V}^T = \mathbf{V}^{-1}$. Also, the square root of the eigenvalues are the singular values along the diagonal of the Σ matrix (Coombe, 2006) .

2.2.2 Tasselled cap transformation

The idea of defining a new coordinate system for the multispectral remote sensing image is applied to develop another group of methods in which new axes are defined in a way that specific information is highlighted in the transformed dataset. To extract physical characteristics from the spectral features and also compressing the various spectral bands to reasonable number of features, understanding the relationship between different bands and interested objects are needed (Crist and Cicone, 1984).

The *tasselled cap* transformation introduced by Kauth and Thomas (1976) is a means for highlighting the most important phenomena of crop development. This transformation is a conversion of the original spectral bands into a new set of bands defined useful interpretations for vegetation mapping. The first tasselled-cap band corresponds to the overall brightness of the image. The second tasselled cap band corresponds to greenness and is typically used as an index of photosynthetically-active vegetation. The third tasselled cap band is often interpreted as an index of wetness of soil or surface moisture. For hydrological applications, the third band is very useful as it emphasizes the water content on the image. Although this transformation produces the same number of output bands as input bands, like PCA, not all of the tasselled cap output bands will be useful. In most cases, the first three tasselled cap bands contain most information from the image and the remaining bands are considered as the noise of the image and are not used. The transformation is known as tasselled cap because of the its shape when the red band values of pixels were plotted against the near infrared pixel values then the coefficients are defined against this graph to maximize the separation of the different growth stages of wheat. The transformation was first introduced for Landsat MultiSpectral Scanner (MSS) in Kauth and Thomas (1976). They assume that KT is a fixed affine transformation,

$$\mathbf{W} = \mathbf{C}\,\mathbf{X} + r \tag{2.13}$$

where $\mathbf{X}$ is the Landsat MMS image bands reshaped as a 2 dimensions vector like previous section. $\mathbf{W}$ is the transformed product, $\mathbf{C}$ is the transformation matrix contains the coefficients and finally r is an offset vector introduced to avoid negative values in the final product. The C matrix contains four unit vectors which are orthogonal to each other. Based on Figure 2.1, the first row of the this matrix C_1 is defined to point along the major axis of soil. This vector is called the soil brightness unit vector. C_2 is chosen to in a way that orthogonal to C_1 and toward the green stuff. C_2 was generated using the Gram-Schmidt orthogonalization procedure. C_3 is chosen orthogonal to both C_1 and C_2 point toward yellow staff using Gram-Schmit procedure. The last vector of C is defined like the previous ones and called non-such.

Following this strategy, Crist and Cicone (1984) developed a physically-based transformation for Landsat TM. Brightness, greenness and wetness are the main three components of their TM Tasselled cap. Now it is available for other popular multispectral optical satellite systems such as MODIS, IKONOS, and QuickBird. So,

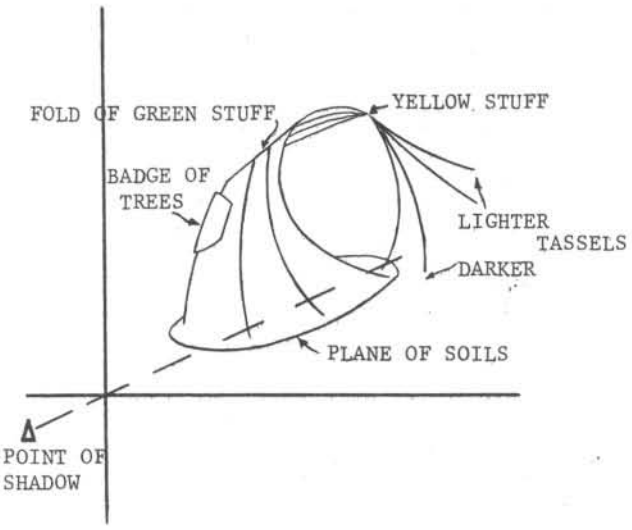

Figure 2.1: The tasselled cap (Kauth and Thomas, 1976)

Kauth-Thomas transformation (KT) provides the opportunity to analytically compare land-cover features directly using satellite imagery from different sensors.

Also KT transformation provides a way to detect and compare changes in vegetation, soil, water content and man-made features over time periods. Finally it is helpful to compress the amount of data from several multispectral bands to three primary components and to reduce atmospheric influences and noise components in images.

2.3 Canonical correlation analysis

CCA is a way of measuring the linear relationship between two multidimensional variables. CCA can find two sets of basis vectors such that the correlations between the projections of the variables onto these basis vectors are mutually maximized. The first linear combination with the largest correlation is called the first canonical variate. The second two linear combinations have the biggest correlation in a way that they are orthogonal with the first pair. This condition must be satisfied by the other pairs as well. An important property of canonical correlations is that they are invariant with respect to affine transformations of the variables. This is the most important difference between CCA and ordinary correlation analysis which highly depend on the basis in which the variables are described (Borga, 1998).

CCA was developed by Hotelling (1936) and now is widely applied not only in statistical analysis but also in economy or medical sciences. Nielsen (1995); Nielsen et al. (1998) firstly applied this technique for change detection. Since then, iteratively

reweighted modification of MAD transformation (IR-MAD) to identify significant change while the area subject to large seasonal changes like vegetation was introduced in Nielsen (2007*b*). The following procedure is suggested to find the nontrivial change between to images acquired in different time from the same area.

To define the canonical correlation between two data set we follow the procedure introduced in Nielsen (1995). To do this, we select two multispectral images from the same area at different time with k spectral bands each of which has p rows and q columns. Again, images in all bands are reshaped as a single column vector in which the number of line represents the total amount of pixels in an image($p \times q$).

$$\mathbf{X} = [x_1, x_2, ..., x_k]^T \quad , \quad \mathbf{Y} = [y_1, y_2, ..., y_k]^T \tag{2.14}$$

We can rewrite $\mathbf{X}$ and $\mathbf{Y}$ as a single matrix partitioned into two groups following:

$$\mu = \begin{bmatrix} \mu_{\mathrm{x}} \\ \mu_{\mathrm{y}} \end{bmatrix} \ , \ \Sigma = \begin{bmatrix} \Sigma_{\mathrm{xx}} & \Sigma_{\mathrm{xy}} \\ \Sigma_{\mathrm{yx}} & \Sigma_{\mathrm{yy}} \end{bmatrix} \tag{2.15}$$

In this equation μ is the mean of the matrices and Σ contains variance and covariance variables. Σ_{xx} and Σ_{yy} are the variances of $\mathbf{X}$ and $\mathbf{Y}$, $\Sigma_{xy}(\Sigma_{yx})$ is the covariance between them. We assume that all elements of Σ are not singular and also $E(\mathbf{X}) = E(\mathbf{Y}) = 0$. Here, we are looking for a linear combinations between $\mathbf{X}$ and $\mathbf{Y}$ like

$$\mathbf{U} = a^T\mathbf{X} = a_1x_1 + a_2x_2 + ... + a_kx_k \tag{2.16}$$

$$\mathbf{V} = b^T\mathbf{Y} = b_1y_1 + b_2y_2 + ... + b_ky_k \quad , \tag{2.17}$$

to maximize their correlation between $\mathbf{U}$ and $\mathbf{V}$ by knowing that $\mathrm{var}(\mathbf{U}) = a^T\Sigma_{\mathrm{xx}}a$, $\mathrm{var}(\mathbf{V}) = b^T\Sigma_{\mathrm{yy}}b$ and $\mathrm{cov}(\mathbf{V}, \mathbf{U}) = a^T\Sigma_{\mathrm{xy}}b$.

$$\rho = \mathrm{corr}(\mathbf{U}, \mathbf{V}) = \frac{\mathrm{cov}(\mathbf{U}, \mathbf{V})}{\sqrt{\mathrm{var}(\mathbf{U})\mathrm{var}(\mathbf{V})}} = \frac{a^T\ \Sigma_{\mathrm{xy}}\ b}{\sqrt{a^T\ \Sigma_{\mathrm{xx}}\ a\ b^T\ \Sigma_{\mathrm{yy}}b}} \tag{2.18}$$

If a and b are the solutions which maximize the correlation, Lagrange multipliers $\lambda/2$ and $\nu/2$ are introduced to define the cost function

$$F = a^T\Sigma_{\mathrm{xy}}\ b - \frac{\lambda}{2}(a^T\ \Sigma_{\mathrm{xx}}\ a - 1) - \frac{\nu}{2}(b^T\ \Sigma_{\mathrm{yy}}\ b - 1) \tag{2.19}$$

By finding $\partial F/\partial b = 0$ and $\partial F/\partial a = 0$, the cost function is maximized and a and b solved and the result is inserted to develop ρ^2

$$\rho^2 = \frac{a^T\ \Sigma_{\mathrm{xy}}\ \Sigma_{\mathrm{yy}}^{-1}\ \Sigma_{\mathrm{yx}}\ a}{a^T\ \Sigma_{\mathrm{xx}}\ a} \quad = \quad \frac{b^T\ \Sigma_{\mathrm{yx}}\ \Sigma\mathrm{x}\mathrm{x}^{-1}\ \Sigma_{\mathrm{xy}}\ b}{b^T\ \Sigma_{\mathrm{yy}}\ b} \tag{2.20}$$

or

$$\Sigma_{xy}\,\Sigma_{yy}^{-1}\,\Sigma_{yx}\,a = \rho^2\Sigma_{xx}a \tag{2.21}$$
$$\Sigma_{yx}\,\Sigma_{xx}^{-1}\,\Sigma_{xy}\,b = \rho^2\Sigma_{yy}b \quad . \tag{2.22}$$

At the end, the desired projection for $\mathbf{U} = a^T\mathbf{X}$ are given by the eigenvectors a_1, a_2, ..., a_k corresponding to the generalized eigenvalues $\rho_1^2 \geq \rho_2^2 \geq ... \geq \rho_k^2$ of $\Sigma_{xy}\Sigma_{yy}^{-1}\Sigma_{xy}$ with respect to Σ_{xx}. Similarly, desired projections of $\mathbf{V} = b^T\mathbf{Y}$ by considering the conjugate eigenvectors b_1, b_2, ..., b_k of $\Sigma_{xy}\,\Sigma_{xx}^{-1}\,\Sigma_{yy}$ with respect to Σ_{yy} corresponding to the same eigenvalues. Now we are able to determine the respective canonical variates for each eigenvalue.

$$\mathbf{U}_i = a_i^T\mathbf{X} \quad , \quad i = 1, ..., k \tag{2.23}$$
$$\mathbf{V}_i = b_i^T\mathbf{Y} \quad , \quad i = 1, ..., k \tag{2.24}$$

2.3.1 Multivariate alteration detection transformation

To highlight the area where maximum change occurs between two images, multivariate alteration detection (MAD) was applied. The name, MAD, is chosen due its application in change detection in remote sensing (Nielsen, 1995). MAD transforms two sets of multivariate data (multispectral satellite images) into a number of differences between two linear combinations of original spectral bands in a way that the maximum change is explained by the first MADs.

Analysing the difference of two images is a common way to detect change. Pixels with zero or low absolute value represent non-change area and pixels with high absolute value demonstrate change. Two images are again reshaped like equation (2.14), now a simple subtraction operator is applied to them

$$\mathbf{X} - \mathbf{Y} = [x_1 - y_1, x_2 - y_2, ..., x_k - y_k]^T \tag{2.25}$$

If the images have more than three bands, it is not possible to visualize changes in all bands. Moreover selecting just three bands among them is not a wise choice. To overcome this problem and to highlight changes in different spectral bands, a linear transformation that will maximize a measure of change like variance can be used. If we assume that the variance of the variables are equal to the unit, then this procedure led to finding principal components of the simple image difference. This technique is highly vulnerable to differences of scale and offset in every individual spectral bands. Another approach to describe the change is described in Fung and Ledrew (1987). They defined certain base for different number of spectral bands

$$a_i^T\mathbf{X} = a_1x_1 + a_2x_2 + ... + a_kx_k \tag{2.26}$$
$$b_i^T\mathbf{Y} = b_1y_1 + b_2y_2 + ... + b_ky_k \tag{2.27}$$

and then apply PCA on their difference to find a and b coefficients. A more efficient approach is to define the coefficients simultaneously by maximizing $\mathrm{var}(a^T\mathbf{X} - b^T\mathbf{Y})$ subject to the constraints that $\mathrm{var}(a^T\mathbf{X}) = \mathrm{var}(b^T\mathbf{Y}) = 1$.

$$\mathrm{var}(a^T\mathbf{X} - b^T\mathbf{Y}) \quad = \quad \mathrm{var}(a^T\mathbf{X}) + \mathrm{var}(b^T\mathbf{Y}) - 2\mathrm{cov}(a^T\mathbf{X}), b^T\mathbf{Y}). \tag{2.28}$$

Then in respect to equation 2.18, we can reshape above equation

$$\mathrm{var}(a^T\mathbf{X} - b^T\mathbf{Y}) \quad = \quad 2(1 - \mathrm{corr}(a^T\mathbf{X}, b^T\mathbf{Y})). \tag{2.29}$$

By looking at this equation, we understand that there must be a positive correlation between a^T and b^T. To highlight the change between two images, a and b must be determined in a way that the variance of corresponding linear combinations must be maximized. It means that we are looking for the coefficients providing minimum positive correlation between $a^T\mathbf{X}$ and $b^T\mathbf{Y}$. To define the coefficients, we apply CCA as it mentioned in the previous section. Finally MAD variables are introduced as:

$$\mathrm{MAD}_i = a_i^T\mathbf{X} - b_i^T\mathbf{Y} \quad i = 1, 2, ..., k \tag{2.30}$$

In this equation, k is equal to the number of spectral bands, a^T and b^T are the vectors derived form CCA. The MAD components are ordered by correlation between pairs. It means that the first MAD shows maximum similarity and minimum change. The second MAD has maximum correlation between pairs subject to the condition that they are uncorrelated with the first MAD component. This condition is valid for other pairs as well.

With $\mathbf{U} = a^T\mathbf{X}$ and $\mathbf{V} = b^T\mathbf{Y}$, define from CCA, the covariance of the MAD components is given by

$$\mathrm{cov}(\mathbf{U}_i - \mathbf{V}_i, \mathbf{U}_j - \mathbf{V}_j) = 2\delta_{ij}(1 - \rho_j) \tag{2.31}$$

where δ_{ij} is Kronecker's delta

$$\delta_{ij} = \begin{cases} 1 & \text{for } i = j \\ 0 & \text{for } i \neq j \end{cases} \tag{2.32}$$

The components are thus orthogonal with variances

$$\mathrm{var}(\mathbf{U}_i - \mathbf{V}_i) = \sigma^2_{MAD_i} = 2(1 - \rho_i)\rho_1^2 \geq \rho_2^2 \geq ... \geq \rho_k^2 \tag{2.33}$$

MAD variates have approximately a Gaussian distribution because of the central limit theorem (Rice, 2006). Also, if there is no change at pixel j, then the MAD values of this pixel have the mean 0. Also, orthogonal MAD variates are independent from each other. So, it is expected that the sum of the squared MAD for each pixel after normalization approximately follows a χ^2-distribution with k degrees of freedom

$$T_j = \sum_{i=1}^{k} \left(\frac{\mathrm{MAD}_{ij}}{\sigma_{\mathrm{MAD}_i}} \right)^2 \sim \chi^2(k) \tag{2.34}$$

This equation can be used to generate a *change / no change* map. For example, we are looking for change areas with 99 % confidence level. Here, assume that the degree of freedom is 7, so the critical value is equal to 18.5. Finally the pixel is tagged as *changed*, if its T value is bigger than 18.5 (2.34). An automatic radiometric normalization for satellite imagery is introduced in (Canty et al., 2004) and (Canty and Nielsen, 2008). As the MAD transformation is invariant to linear transformations, the areas have small MAD values is applied as reference points for the radiometric normalization process. For example, suppose that the degree of freedom is 7 so the critical value for the stable pixels with 99 % confidence is 1.24 . It means that pixels with T value smaller than 1.24 considered as fixed points. For maintaining consistency in the notation with the other sections, we reverse the order of the MAD variables. It means that the first MAD highlights pixels with least similarity and the last MAD represents the constant area.

2.3.2 Maximum autocorrelation factor transformation

To find areas with maximum change, applying a MAF postprocessing of the MAD and PCA variates is suggested. MAF was developed by Switzer and Green (1984). This procedure exploits the fact that in change detection applications of natural phenomena, the intensity of pixels in the image is strongly correlated with neighbouring pixels, while the noise shows only weak spatial correlations. Despite PCA which is maximize the data variance, MAF transformation maximize the autocorrelation of each components. This transformation is equivalent to a transformation to a coordinate system in which the covariance matrix of the spatially shifted image data is the identity matrix followed by principal component transformation (Nielsen, 1995).

Here, we reshape the multispectral image bands in this way:

$$\mathbf{Z}^T = [\mathbf{Z}_1(x), \mathbf{Z}_1(x)..., \mathbf{Z}_k(x)] \tag{2.35}$$

$$\mathbf{E}(\mathbf{Z}(x)) = 0 \tag{2.36}$$

$$\text{var}(\mathbf{Z}(x)) = \Sigma \tag{2.37}$$

In this equation, k is the number of spectral bands, $\mathbf{Z}(x)$ represents image value of the pixel located at $x = [x1, x2]$. Also we introduce a spatial shift $\Delta^T = (\Delta_1, \Delta_2)$ and their covariance function is $\text{cov}(\mathbf{Z}(x), \mathbf{Z}(x + \Delta)) = \Gamma(\Delta)$. This variable has certain properties

$$\Gamma(0) = \Sigma \tag{2.38}$$

$$\Gamma(\Delta)^T = \Gamma(-\Delta) \tag{2.39}$$

Now we try to find a vector basis (a) for $\mathbf{Z}(x)$ in a way that minimize the correlation between $\mathbf{Z}(x)$ and $\mathbf{Z}(x + \Delta)$. So the following equation must be minimize.

$$\text{corr}(a_T\mathbf{Z}(x), a_T\mathbf{Z}(x + \Delta)) = \frac{\text{cov}(a_T\mathbf{Z}(x), a_T\mathbf{Z}(x + \Delta))}{\sqrt{\text{var}(a_T\mathbf{Z}(x))\text{var}(a_T\mathbf{Z}(x + \Delta))}} \tag{2.40}$$

We know that $\text{var}(a_T\mathbf{Z}(x)) = \text{var}(a_T\mathbf{Z}(x+\Delta)) = a^T\Sigma a$ and based on mathematical details in Nielsen (1995)

$$\text{cov}(a_T\mathbf{Z}(x), a_T\mathbf{Z}(x+\Delta)) = a_T(\Sigma - \frac{1}{2}\Sigma_\Delta)a, \tag{2.41}$$

finally by replacing equation (2.41), we reshape equation (2.40)

$$\text{corr}(a_T\mathbf{Z}(x), a_T\mathbf{Z}(x+\Delta)) = 1 - \frac{1}{2}\frac{a_T\Sigma_\Delta a}{a_T\Sigma a}. \tag{2.42}$$

So if we want to minimize the correlation between $a_T\mathbf{Z}(x)$ and $a_T\mathbf{Z}(x+\Delta)$ then $\frac{a_T\Sigma_\Delta a}{a_T\Sigma a}$ must be maximize. If $(\rho_1, \rho_2, ..., \rho_k)$ is the eigenvalues and $(c_1, c_2, ..., c_k)$ is the corresponding eigenvectors of Σ_Δ with respect to Σ, then we assume that:

$$\mathbf{Y}_i(x) = c_i\mathbf{Z}_i(x) \quad \text{where} \quad i = 1, 2, ..., k \tag{2.43}$$

In this equation k is equal to the number of different spectral bands and $\mathbf{Y}$ is the new data set composed of the original data in a way that the first component of it ($\mathbf{Y}_1$) has the biggest autocorrelation factor and the second one ($\mathbf{Y}_2$) has the biggest autocorrelation factor in a way that it is orthogonal to the first one.

In the final product, the area with high spatial correlation with its neighbourhood becomes visible in the first elements of MAF. Applying MAF transformation on MAD variations is a way to highlight the change area and also isolate the noise while MAD variations present different orthogonal linear combination of original bands which have maximum correlation and maf analysis of MADs provides a way to retain the spatial context of neighbourhood pixels in the final change detection product (Nielsen et al., 1998).

Chapter 3

Independent data transformation analysis

In this section, we will focus on methods in which spectral transformation is applied on each image independently. The main aim of this chapter is to reduce the noise level and to highlight the desired physical characteristic of the image. Finally, enhanced images are classified separately and the change is detected by comparing the classified images.

The study area for this chapter is part of Niger river which is described in the first chapter

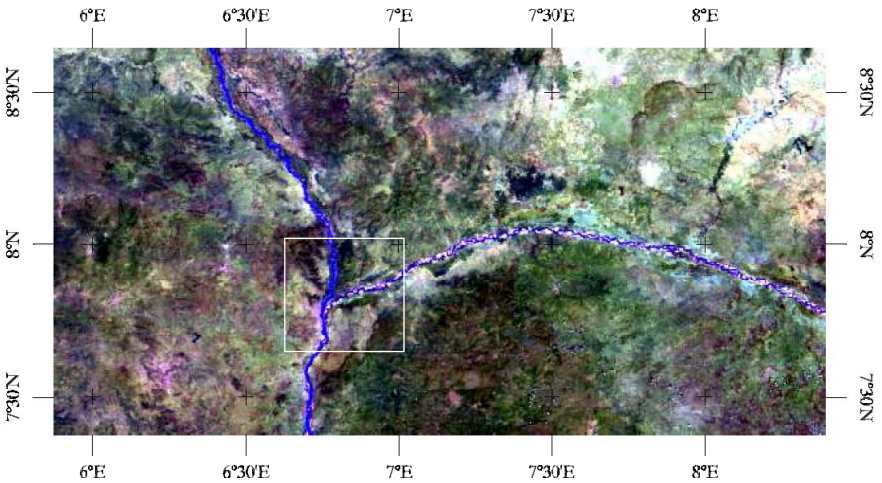

Figure 3.1: A RGB image of Niger delta derived from MODIS mod09

To monitor the change in the river extent during different wet and dry seasons, three MOD09 MODIS images at different date are collected. The images are available in seven bands from visible to near infrared in light spectrum. In Figure 3.2c, RGB image of the river at three different time is presented.

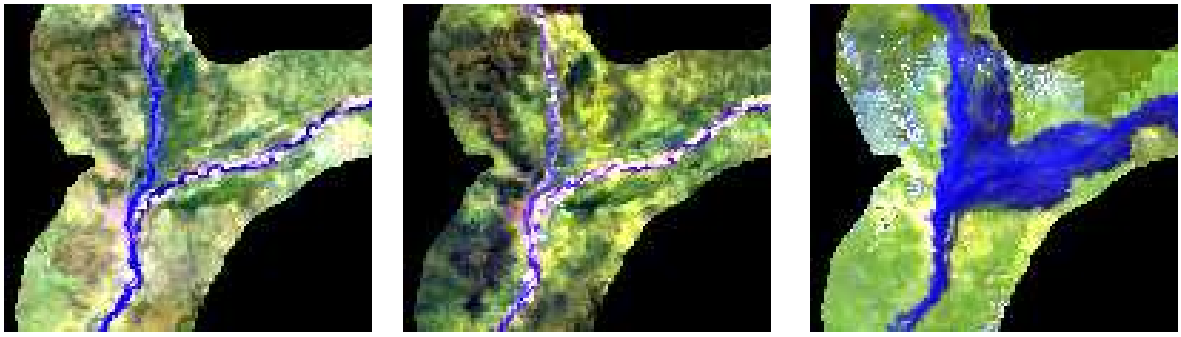

(a) 2012.01.0.1 **(b)** 2012.04.01 **(c)** 2012.09.19

Figure 3.2: RGB image of Niger river derived from MODIS MOD09 at three different epochs

Now, to enhance the quality of images, PCA transformation is applied to each of them separately. The mathematical concept of PCA is described in the previous chapter and Figure 3.3 roughly describes the procedure applied to each image in this section.

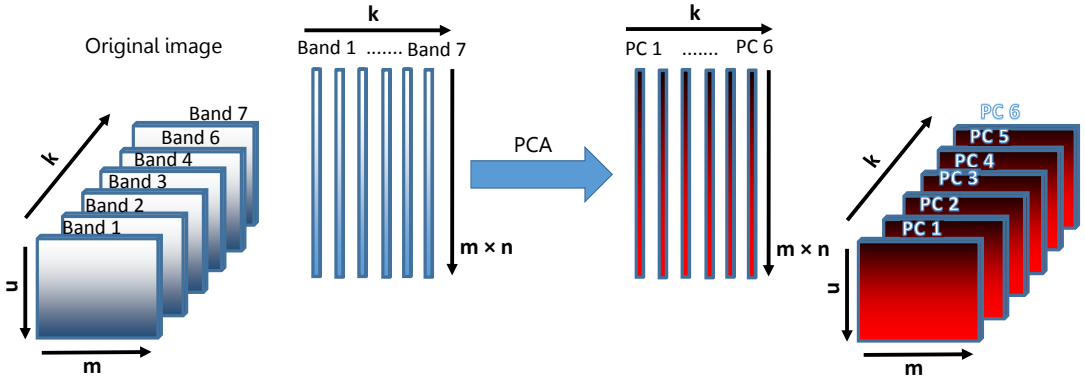

Figure 3.3: Procedure of PCA transformation on a single multispectral image

Based on the algorithm, each image with m columns and n rows in certain spectral band is reshaped as a one column vector. So, a multispectral images with k bands is changed to a two dimension matrix with k columns and $n \times m$ rows. Then, PCA transformation is applied to the reshaped image according to previous section. To evaluate the result of PCA transformation, each PC reshapes to a two dimension matrix again with m columns and n rows. Unlike the original image ordered based on their wavelength, PCs sorted according their importance. It means that the first PC contains the majority of total variance and so on.

Table 3.1: Eigenvalues and their percentage derived from both covariance and correlation matrix

	Covariance		Correlation	
Num	Eigenvalue	Percentage	Eigenvalue	Percentage
1	1.713842	99.95%	3.809813	63.5%
2	0.000618	0.036%	1.732290	28.9%
3	0.000191	0.011%	0.378380	6.3%
4	0.000018	0.001%	0.037291	0.6%
5	0.000009	0%	0.026204	0.4%
6	0.000001	0%	0.016023	0.2%

The routine is applied on all spectral bands of image acquired on January 1, 2012 and in Table 3.1, eigenvalues and eigenvectors derived from covariance and correlation matrix are presented.

Regarding this table, It is obvious in the second and third columns that the majority of the variance concentrates in the first PC (more that 99%). So, the rest of the PCs are hardly containing any information because less than 1% of variance is divided between them. On the other hand when correlation matrix is used to derive PCs, the correlation is shared between all the PCs descendingly.

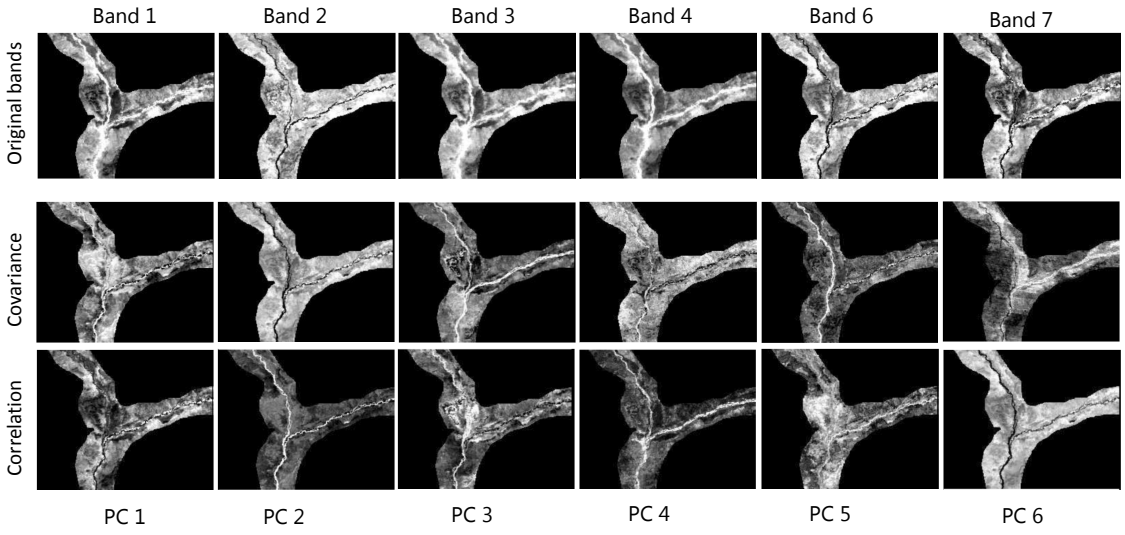

Figure 3.4: Different image bands and PCs derived from covariance and correlation matrices

After calculating PCs, each PC is reshaped to its original dimension. In Figure 3.4, we compare the original image bands with PCs derived from correlation and covariance matrices. Each of the PCs is generated by applying different set of coefficients on image bands, so each of them represents a particular characteristic of the area.

Applying classification methods on PCs directly is not possible because the coefficients are defined based on mathematical process aiming to optimize variance and it is very hard to assign physical characteristics to the PC values. However, certain combinations of different spectral bands with different coefficients could improve our understanding from the image and also make it easier to visually.

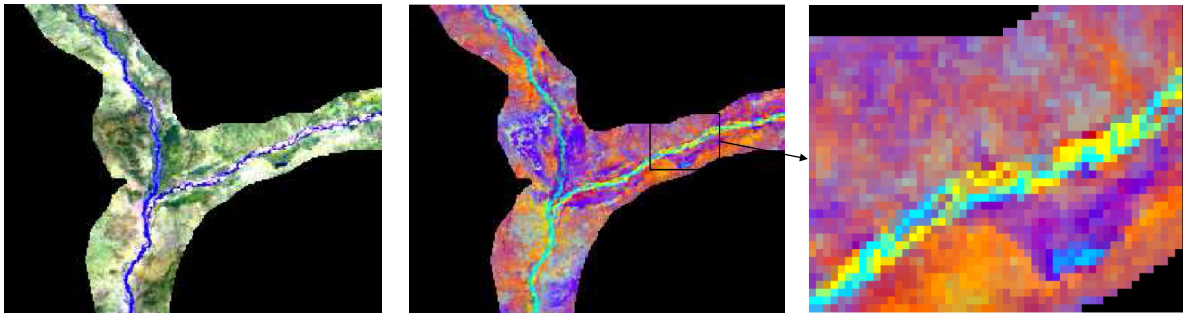

Figure 3.5: (Left) original image. (Center) combination of first three PCs as image bands. (Right) determined area in the center image

As shown in Figure 3.5, it is easier separate the main river margins from the dry lands as they appear red in the images. Also the seasonal behavior of river is detectable while the dry part of river bed looks yellow. It must be mentioned that this interpenetration is not valid before the comparison the product with the original image.

To reduce the noise level of the image and also enhance the quality of it, it is assumed that there is no valuable information in the last three PCs because they contain less than 1% of correlation. The new image is reconstructed by using just first three PCs.

In Figure 3.6, the first three PCs are applied as three different image bands in the second column. As discussed before this way of visualization can help us to interpret easier and also to extract more information. For example, in the last image of the second column, the primary border of the river is recognizable even in the flooded area in addition to distinguish between land and water in general. In the third column, the reconstructed images from just first three PCs is presented. It is obvious that they are more clear than the images in the first column because half of the PCs are removed. In the last column, we can see that there is a clear distinction between water and land because this band is appropriate for this aim and also the noise level is reduced due to elimination of some PCs.

This approach to enhance the quality of the image is just based on mathematical assumptions and does not have any physical constraint. Ignoring the last PCs is not the best strategy while we deal with earth related phenomena as they have special signature on different spectral image bands. Because our decision about selecting the PCs is based on dispersion of pixel values from the mean value of all pixels and also we know that there is a big difference between the value of water and land in the image bands.

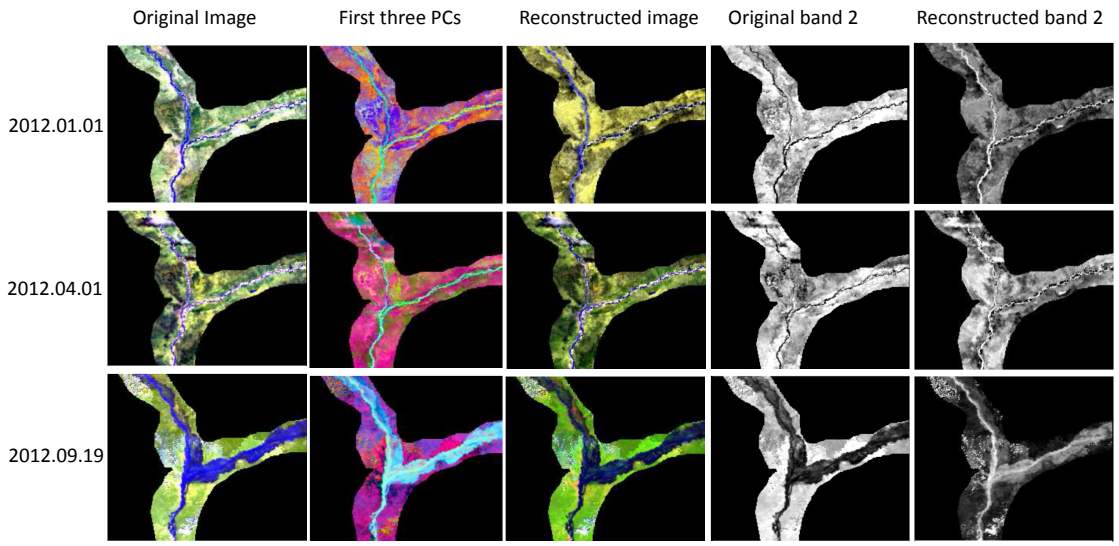

Figure 3.6: Reconstruction of the images to reduce the noise. (First column) original RGB images. (Second column) representation of first three PCs. (Third column) reconstructed images with first three PCs. (Fourth column) original band 2. (Fourth column) original band 2. (Fifth column) reconstructed band 2

Table 3.2: Eigenvectors of all image bands (date: 2012.01.01)

Eigenvector	1	2	3	4	5	6
Band 1	0.462985	0.235730	0.463922	0.427226	0.377357	0.435812
Band 2	0.311621	−0.579566	0.300545	0.387630	−0.490714	−0.292593
Band 3	0.044286	0.735800	0.038738	0.292949	−0.257570	−0.550432
Band 4	0.192765	0.095869	−0.667839	0.344042	−0.409006	0.471159
Band 6	−0.504741	0.170752	0.486356	−0.055782	−0.531191	0.440753
Band 7	−0.628215	−0.169664	−0.101969	0.678178	0.317819	−0.072305

Another strategy to select the PCs is studying the role of different bands in each PC. By looking in eigenvectors, the appropriate PCs is determined by investigating about the information highlighted in each bands.

To select the appropriate PCs for reconstructing the image, we must have a good overview about the data and case study. The images used in this research involve different electromagnetic spectrum from visible till near infrared (Figure 3.7).

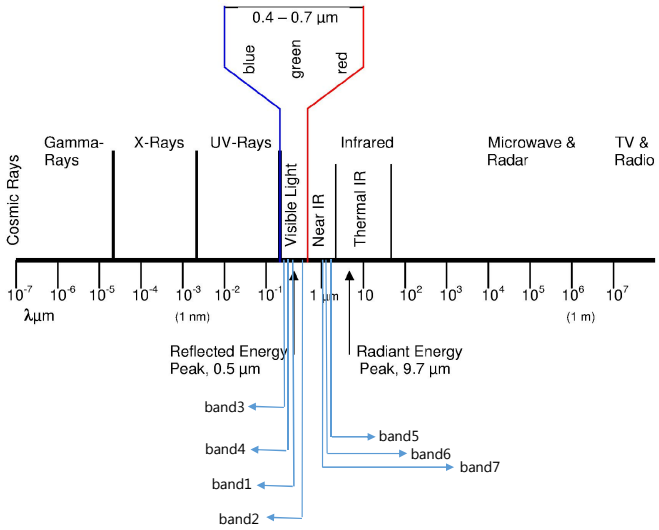

Figure 3.7: A light spectrum and location of different bands

The aim is to highlight different characteristics of the river. In this way, first based on Table 3.3 we can understand that the ability and sensitivity of different bands against water content are different. So, we must decide which spectral bands are the most appropriate for our goal. Then find the most reasonable PCs to reconstruct the image.

Table 3.3: Description of different spectrum bands[1]

Band	Description
1	Useful for distinguishing planet species, as well as soil and geologic boundaries.
2	Useful for detecting water land boundaries. able to penetrate into the haze.
3	Best for mapping depth detail of water covered area.
4	Useful for mapping detail such as depth or sediment in water bodies.
6	Sensitive to plant water content. This band is also used for distinguishing clouds, snow, and ice.
7	Responsive to plant and soil moisture content.

With respect to Table 3.3 we can conclude that bands 2, 3 and 4 contain the most important information to monitor the change in water extent and also water area. Band 2 is best for detecting water land boundary which is our main concern. Also, the tiny part of sunlight which can slightly penetrate in to the water column is observed in band 3 and 4. So, PCs in which these bands have bigger coefficients are selected and we assume that these linear combinations retrieve more information about the river.

[1] `yale.edu/ceo/Documentation/guide_text.html`

By looking again at Table 3.2 for this image, we decided to keep just PCs number 2, 3 and 6 to reconstruct the image while their linear combinations of different spectral bands highlight the characteristic of water body.

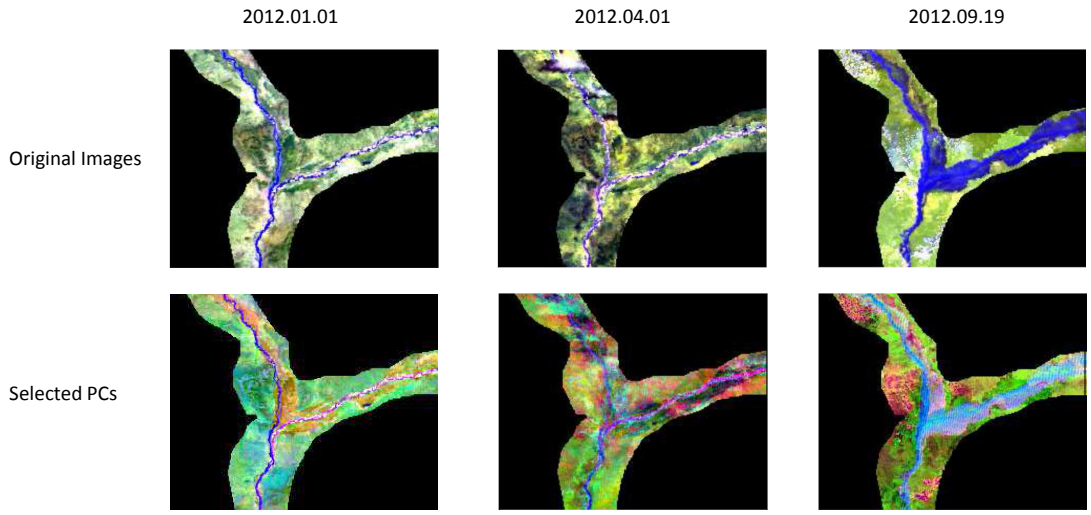

Figure 3.8: Comparison of original images and images generated by three selected PCs

As presented in Figure 3.8, this strategy is applied to all three images. The second row of this figure indicates that more detail of river and surrounding area are highlighted. In this figure, we can see that the river boarders are easily separable. By looking carefully at the last one, we can find that the main river boarder is detectable form the flooded area as the flooded area is presented in pink.

There is still a lot more information that we can obtain form the images. For example by looking carefully at Figure 3.8, it is clear that the left part of the river appears blue (as it is expected) but the right part of river appears pink. The reason of this difference in color will be investigated by looking at the pixel values at two points in these areas.

By comparing the values of two pixels in figure 3.9, we understand that the difference of values in PC6 and especially in PC2 is the reason of this difference in color. By looking at Table 3.3 and Table 3.2, we can conclude that change in the river depth is responsible for this change in color. But, without any external source of information, we can't define which part of river is deeper than the other part.

The idea of highlighting specific physical characteristics of images leads us to apply the tasselled cap transformation described in the previous section on them. For hydrological purposes, the wetness component gathers all information about water content and soil moisture in all spectral bands. In the Table 3.4 , the coefficient of this

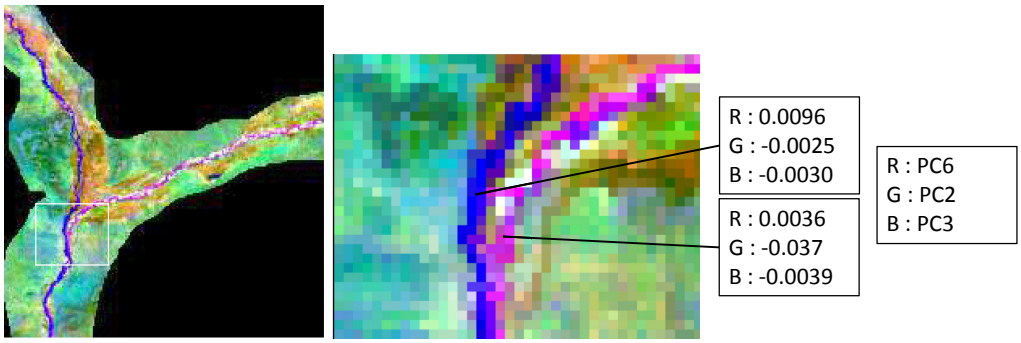

Figure 3.9: Comparison of two pixels values to find the change

transformation for the Landsat 7 images are presented.

Table 3.4: Coefficients of Kauth-Thomas Tasselled Cap Transformation for LandSat 7 image

Index	Band 1	Band 2	Band 3	Band 4	Band 5	Band 6
Brightness	0.3561	0.3972	0.3904	0.6966	0.2286	0.1596
Greenness	−0.3344	−0.3544	−0.4556	0.6966	−0.0242	−0.2630
Wetness	0.2626	0.2141	0.0926	0.0656	−0.7629	−0.5388
Fourth	0.0805	−0.0498	0.1950	−0.1327	0.5752	−0.7775
Fifth	−0.7252	−0.0202	0.6683	0.0631	−0.1494	−0.0274
Sixth	0.4000	−0.8172	0.3832	0.0602	−0.1095	0.0985

Figure 3.10 presents the coefficients applied to different bands of Landsat 7 image. The river and its border are clearly detectable in the wetness component. It is a prominent sign for water extent monitoring as there is a high contrast between water and land in this component. Clouds, as one of the main sources of error in this category, appear dark in the wetness component. So unlike infrared bands, separation between water and clouds is possible in this component.

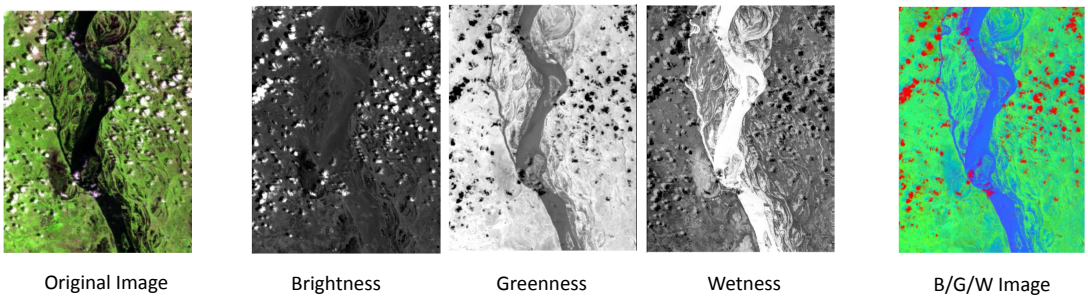

Figure 3.10: Result of Tasselled Cap transformation on a LandSat 7 image

In this chapter, PCA transformation is applied in multispectral image mainly to reduce the noise level in the image. The way that PCs selected for reconstructing the

image is critical. Here we indicate that having knowledge about research aim and also data lead to better strategy for picking up appropriate PCs. KT transformation directly changes spectral bands to the physical based parameters and provides a numerical way to compare different images. Also, representing PCs instead of original spectral bands in image color bands is a fascinating technique to extract more information form an image.

Chapter 4

Merged data transformation

In this chapter, we will focus on methods in which multispectral transformations are applied to more than one image simultaneously for the purpose of change detection using the transformed images. In the first section, we evaluate change detection methods based on CCA and in the second section PCA is applied on merged multitemporal images to enhance the change between two images.

4.1 MAD and MAF analysis

Analysing the change in multitemporal images is not possible unless some image preprocessing is applied. Among them, geometrical rectification, image registration and radiometric, atmospheric correction and topographic correction (specially mountainous regions) are necessary. Advanced optical systems like MODIS and Landsat provide relatively precise geolocation information with their products as long as they compare with themselves there is no need for applying geometric and image registration. Maintaining radiometric consistency between multitemporal images is not possible due to different atmospheric conditions, variations in the solar illumination angles and sensor calibration trends (Du et al., 2002). Most of the solutions are suggested based on the assumption that the relationship between the radiance recorded at two different times from a same region can be approximated by a linear function. In addition to refining images before analyzing the change, we can apply change detection techniques which are invariant to affine transformations (including linear scaling). Both MAD and MAF variates have this property which means that they are not sensitive to offset and gain between multitemporal image bands (Nielsen et al., 2002). So by taking advantage of these methods, we are confident that the real change due to different environmental patterns will be extracted without any preprocessing

In this section, two Landsat 8 images with 30 meter pixel size of Niger river from different epochs are used as case study. We apply MAD and MAF transformation to the original image bands. Unlike MODIS products, Landsat images need a careful consideration before comparing them together. So, applying MAD and MAF transformations

for change detection could be an alternative to cumbersome radiometric calibration and normalization process.

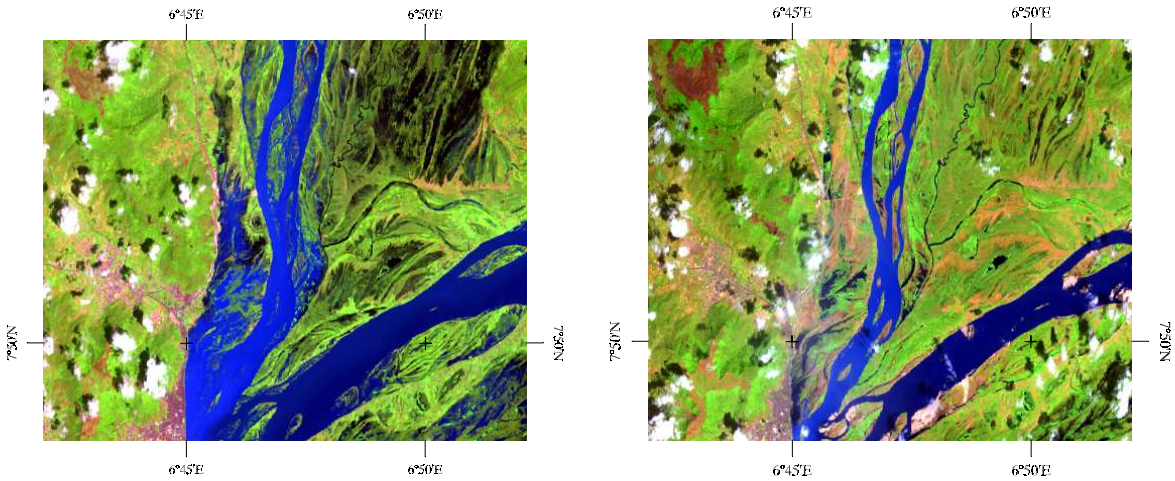

(a) Date: 2013-10-17 **(b)** Date: 2013-11-18

Figure 4.1: Part of Niger river form Landsat 8

As shown in Figure 4.1, a significant change in river extent and wetland occurred during one month. Also the pattern of vegetation changed especially in the north west of the image. As we expected, clouds covered parts of both images which may affect the change detection process. We expect that change in the river extents will become visible in the last MADs because they are the most dominant change during the time. On the other hand, the change in cloud cover will affect the last MADs. Figure 4.2 illustrates the procedure of this transformation. In this figure, n is the number of rows and m is the number of columns in each spectral image, k is also the number of different spectral bands.

To detect the change between to images, we generate a map based on equation (2.34). As discussed before, we assume that MAD components follow a χ^2 distribution, here with seven degrees of freedom. Figure (4.3) represents the probability of change in the characteristic for each pixel. Based on this distribution, the possibility of change in pixels with a value less than 1.96 is approximately about 2.5 % and they illustrate in dark blue color in the figure. As well as, this possibility in pixels with the value approximately bigger than 25 is about 99.9 % . As we expected, the change in the river boundary in the middle of the image is highlighted. Unfortunately, the change in cloud patterns between two images spoils the result because this change is dominant in every spectral band so we can see them all over the image.

Analysing each MAD separately to detect the change is another way that we can apply this transformation for our purposes. The first MAD highlights the area that significant change occurred because the maximum spread in the pixel intensity occurred on that

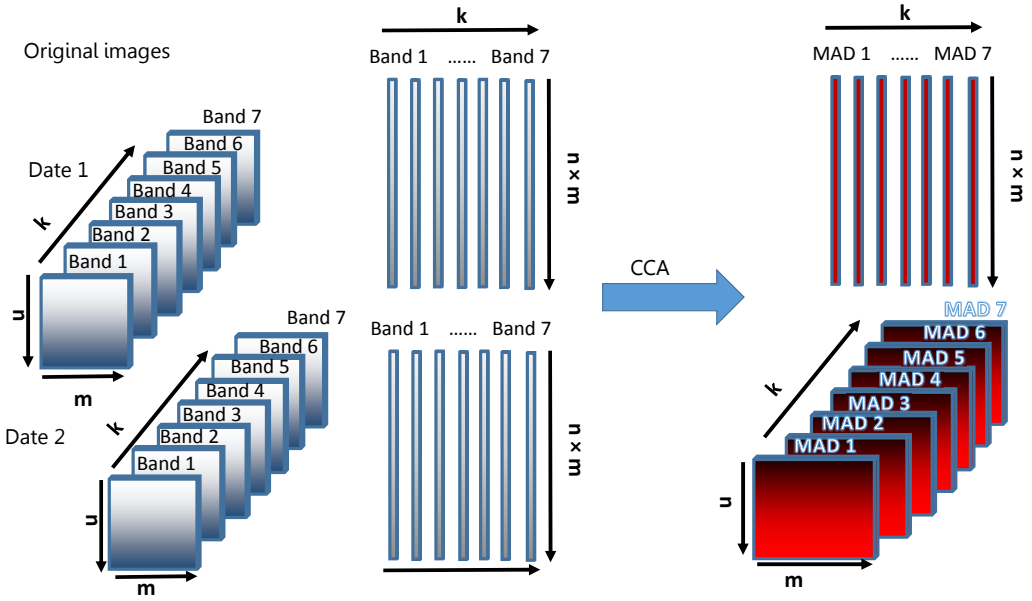

Figure 4.2: Procedure of applying MAD transformation on multitemporal images

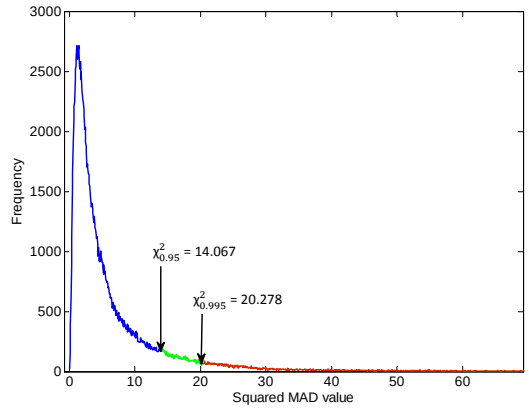

(a) Histogram of the image

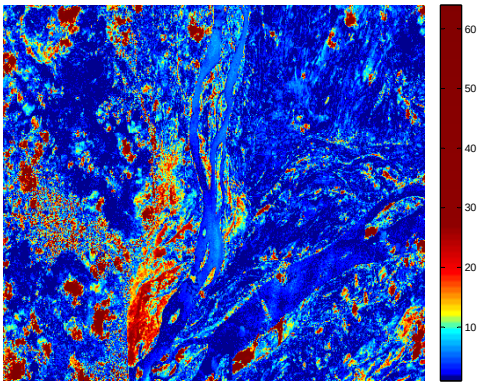

(b) Summation of the squared MADs

Figure 4.3: Map of the summation of the squared MAD values per pixel corresponding to test statistic (equation 2.34)

area. The second MAD also carries important information about the change because it has maximum variance but subject to this condition that it is uncorrelated with the first one. Other MADs are also arranged in a way that they are uncorrelated with each other and the variance between to linear combinations is descending from last MAD to first one (Figure 4.5).

As we described before, it is expected that the map of the two or three first MADs cover the change in multitemporal images. In Figure (4.5), all MADs are presented. In MAD 1, the main part of river appear black because it remain stable during the time and the

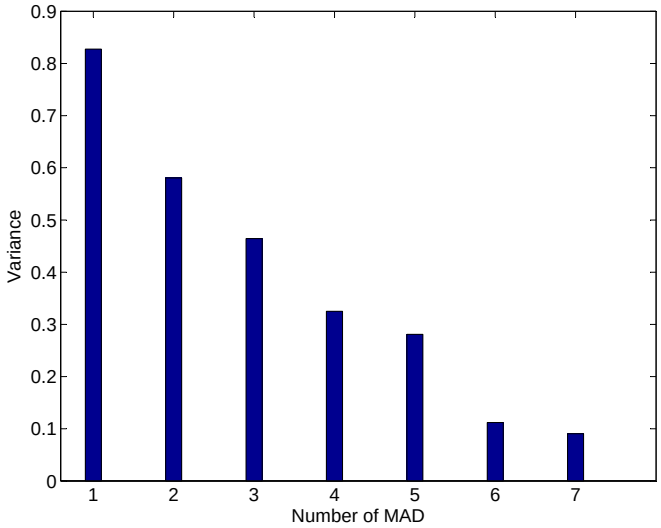

Figure 4.4: Variance of the MAD components

flooded area appears white as the most intense change from wet to dry land. Different gray levels indicate the change in type and density of vegetation. It is interesting that the boundaries of stable part of river and also the flooded area are clearly distinguishable. By looking at all MADs, we conclude that there is no valuable information on the change in the last four MADs. Last MADs contain the noise component and also trivial change.

Based on the assumption that there is no valuable information in the last four MADs, we can combine the remaining three MADs as different color bands of a RGB image. This image might help us to better understand and interpret the physical characteristics of the river and the area around at both epochs and also the change occurred during the time. Inspection of Figure 4.6 and comparison with Figure 4.1 give us a novel basis for interpretation.

In Figure 4.6 the part of the river that is consistent in both acquisition dates are shown in dark blue. Yellow indicates the area that was covered by water in the first and dry in second images. Areas with little change are presented in light blue and green. Finally, the change in vegetation type and intensity are presented in black and red. Unfortunately, the change in the clouds cover reduces the quality of the result for example in the right branch of the river. It is obvious that how clouds affect MADs.

MAD variables provide valuable information, nevertheless in the first MADs we see that they are partially saturated by the noise. Specifically, the parts that minor change in vegetation is occurred. In Figure 4.6, the left side of the river appears noisy because the level of change is negligible in respect to the the other part. Also we know that physical objects observed in the images occupy several pixels. If a change will occur on them, it must follow a physical pattern. So, applying MAF transformation to highlight areas with high spatial autocorrelation will effectively improve the final

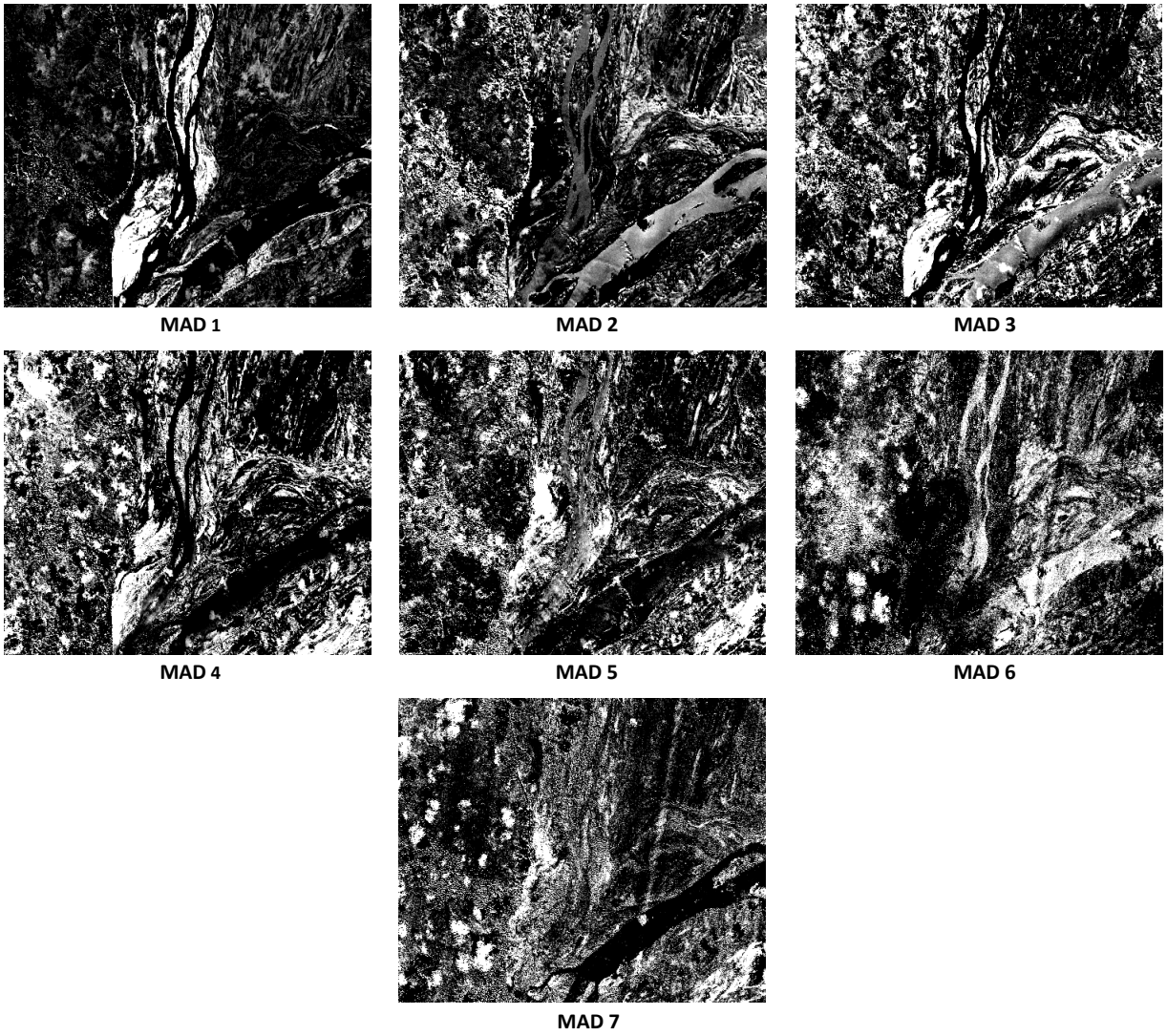

Figure 4.5: MAD components of the two images

result. If the MAF transformation is applied to the MAD components, the real change in the physical condition with high spatial correlation is determined.

In Figure 4.8, as it is expected, in the first and the second MAFs, changed area with high correlation is clearly recognized. Like MADs, here also after third MAF, there is no valuable information about change and the last two MAFs are mostly covered with noise. Like before, to improve our interpretation, we can put the first three MAFs contained the most information in different color channel of a RGB image.

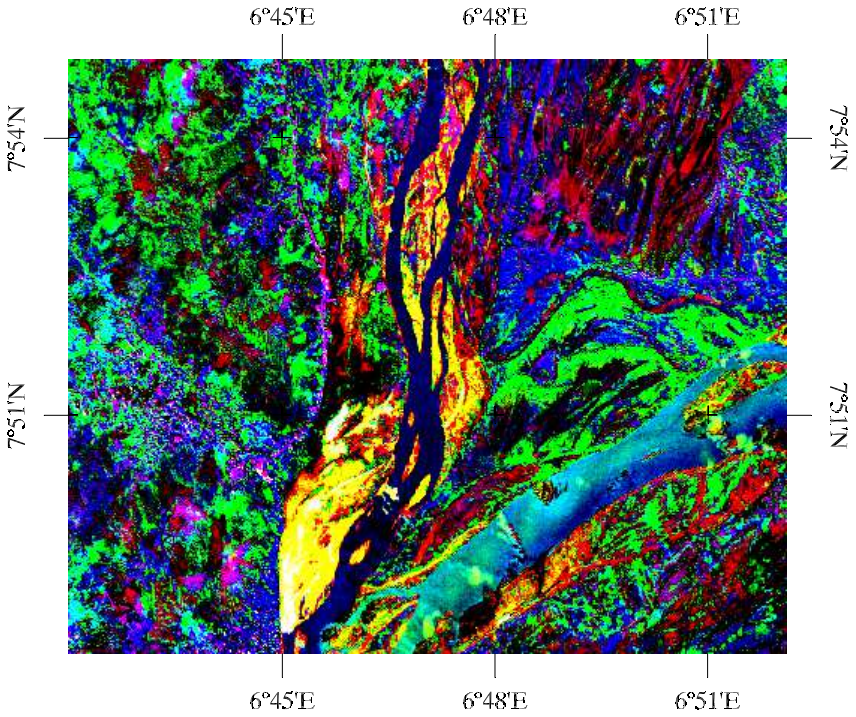

Figure 4.6: Color composite of the last three MAD (Red: MAD2, Blue: MAD1, Green: MAD3)

Figure 4.8 is clearly improved visually with respect to Figure 4.6. In this figure, dark and light blue indicate the not change area. Area covered with water in the first image and dry in the second one are shown by yellow, green and also red. Black especially in the upper part of the image represents the change in the vegetation. Reduction of the noise is the most significant improvement in this figure. Unlike MAD analysis, here we deal with a very clear image which is very easy to interpret. For example, in the left part of the image, even clouds are apparent pink. This is something that is not visible in the MADs.

In Figure 4.9, normal difference of two RGB images, color composition of first three MADs and combination of first three MAFs are shown to illustrate the improvement in each step. In the figure (a), finding the changed area is not easily possible because two images do not have the same origin and scale. Also selecting just three spectral bands out of seven is a hard decision while in the original image, bands just ordered based on their spectral range. So three spectral bands must be selected based on visual interpretation, here we choose band 6 , band 5 and band 4. Figure (b) provides more valuable information about the change because in each MAD, a linear combination between different bands try to maximize variance and highlight the change . More than it in figure (c), the spatial correlation between neighbouring pixels are maximized. So, the comparison between figure (a) and (c) shows the ability of MAD transformation to capture the real change and also reorder the image bands based on their importance. Also, MAF transformation keeps the coherency of changed area and in the first MAFs,

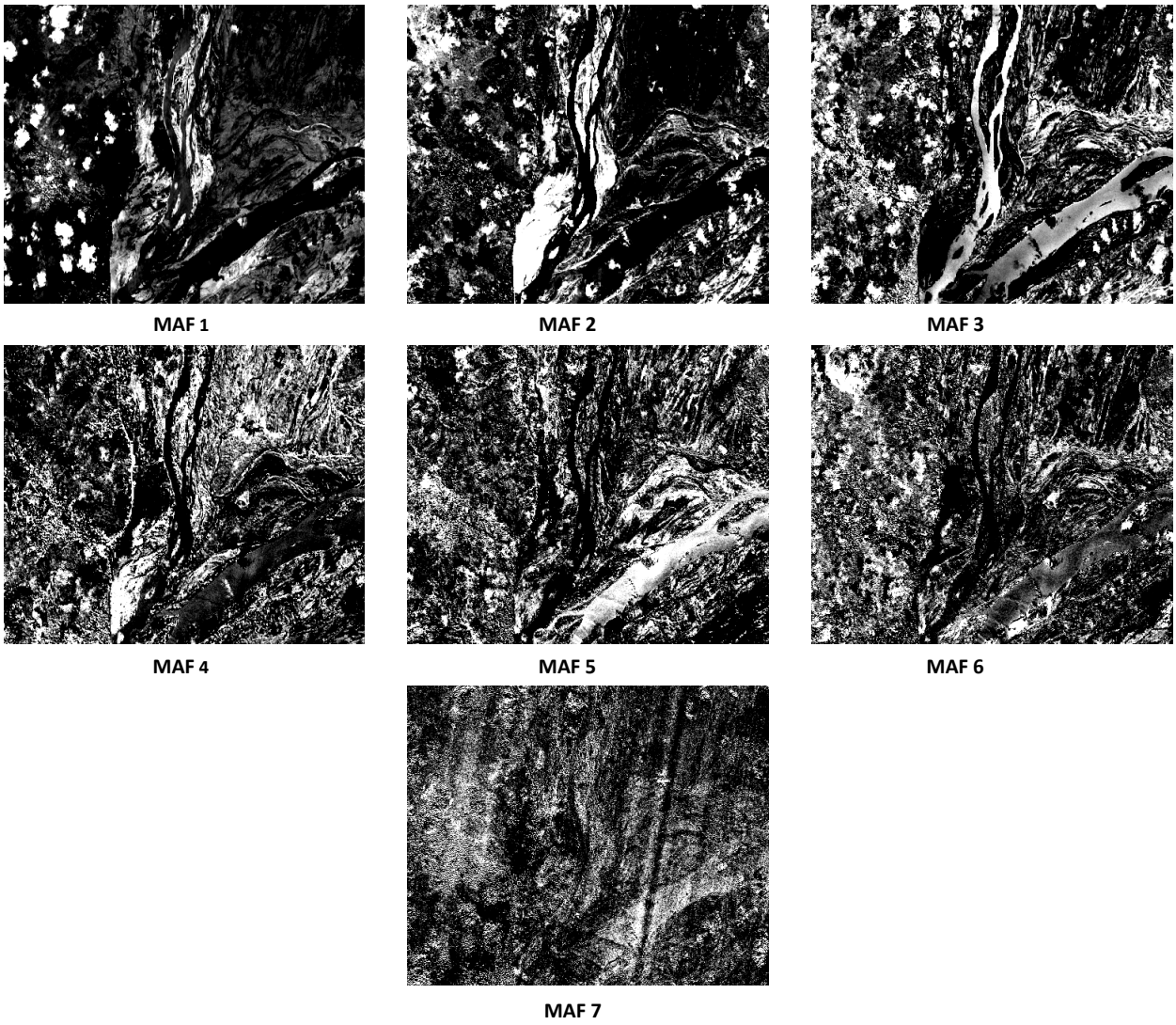

Figure 4.7: MAF of the MAD components

the area with high spatial correlation are highlighted.

4.2 Principal component analysis

In this section, three different techniques based on PCA for change detection will be applied. First, two multitemporal images merge into a single image after which PCA is applied. Second, an image difference generated from two images will be enhanced by PCA. Third, PCA is applied to a number of images from a river section to reduce the noise. For the first two experiments, two images from the previous chapter are selected (Figure 4.11). In these images, A significant change in the river extent and

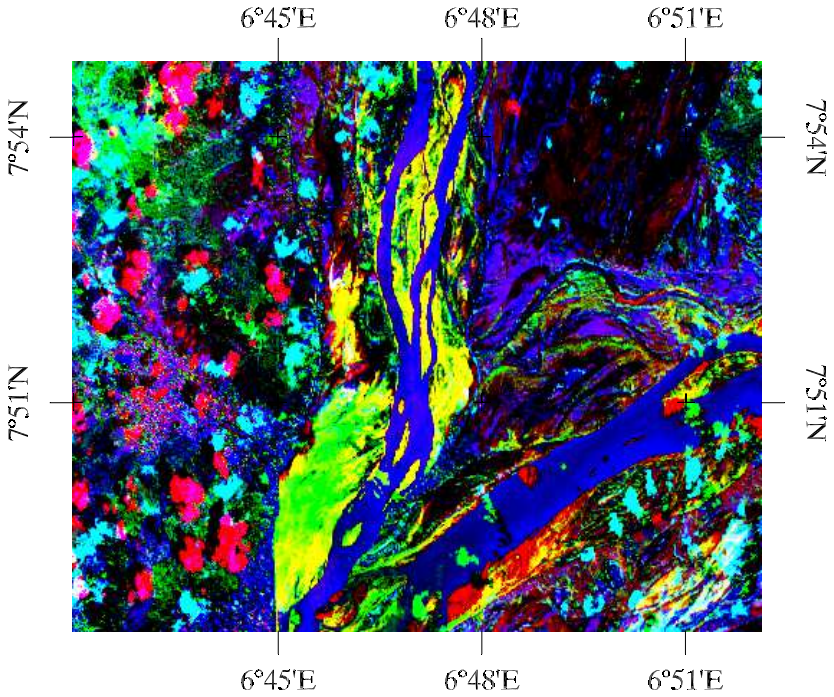

Figure 4.8: Color composite of the last three MAF (Red: MAF2, Blue: MAF1, Green: MAF3)

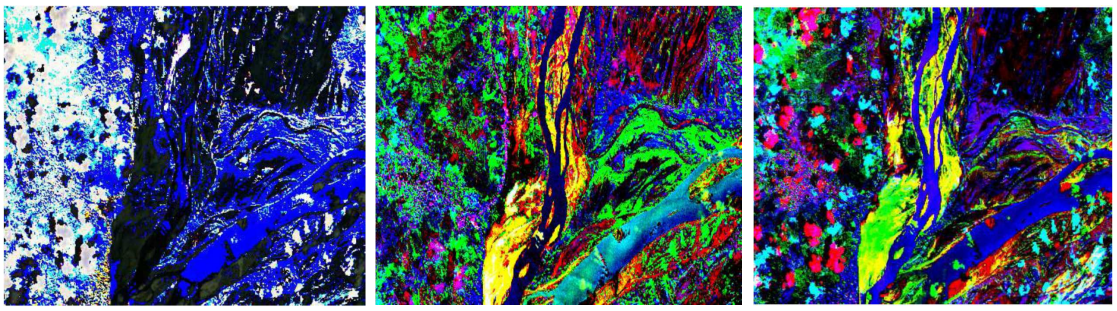

Figure 4.9: a) Ordinary difference of bands 6, 5 and 4 b) color composite of MADs, c) color composite of MAFs

flooded area are happened between two epochs.

Based on Figure 4.11, all different spectral bands from two multitemporal images are registered and treated as a single N - dimensional data set as input to PCA. After applying PCA, each PC must reshape to the original dimensions. Now the main concern is selecting appropriate PC to describe and analyse the situation of each image and also the occurred change. In other words, PCA is applied here to isolate the noise component of the images and also to highlight the change between multitemporal images especially visually.

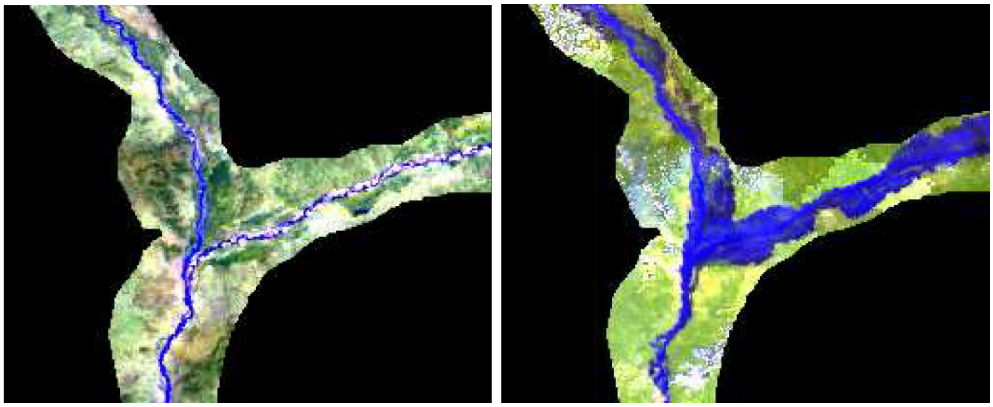

Figure 4.10: Niger River, left (2012.01.01), right (2012.09.19)

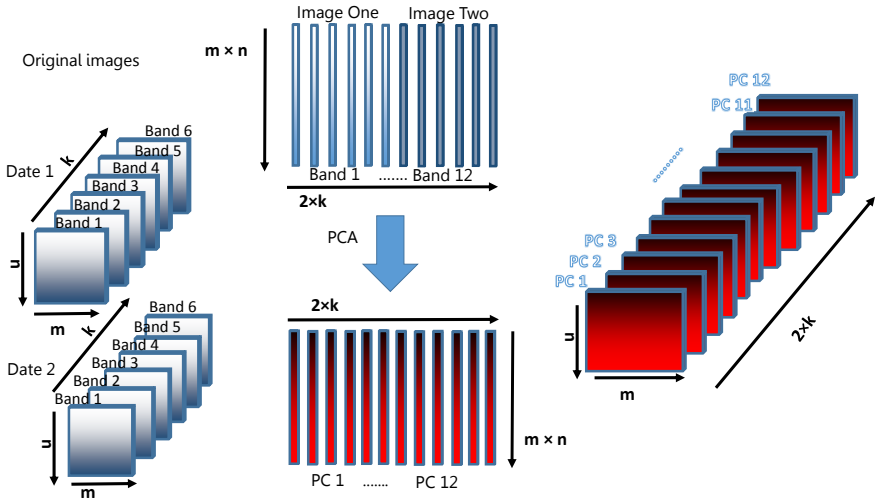

Figure 4.11: Procedure of applying PCA on multitemporal images

To select the appropriate PCs, we can not simply choose the primary ones because here the definition of correlation (covariance) is completely different from previous examples. Here, correlation (covariance) matrix represents the difference from the mean pixel value among each image bands and also between two multitemporal images. So, picking the primary PCs for interpretation is not the solution because they are ordered based on their variance portion. In this way, PCs must be chosen very carefully by investigating the eigenvectors. To do this, first we must define the phenomena that we have aim to monitor it e.g. river extend, flooded area. Then based on Figure 3.7 and table (3.3), finally PCs in which the most appropriate image bands from both images have noticeable coefficients are selected for present them as RGB image.

From the previous section, we learn that most of the important information for our purposes concentrates in band 2, band 3 and band 4. So among all PCs, we are looking

Table 4.1: Eigenvectors of combination of two multispectral image bands PC1 to PC6

Eigenvector	1	2	3	4	5	6
Band 1	−0.438684	−0.252837	−0.441010	−0.389075	−0.401970	−0.451105
Band 2	−0.103324	0.050066	−0.100850	−0.157657	0.055271	0.032167
Band 3	0.195323	−0.164536	0.184407	0.276605	−0.205160	−0.113435
Band 4	−0.264132	0.625614	−0.262364	−0.239288	0.387361	0.192283
Band 6	0.091844	0.668214	0.097280	0.260711	-0.286185	−0.587742
Band 7	0.064112	−0.030757	0.039499	−0.061921	0.045988	0.050121
Band 1	−0.057235	0.002719	−0.197143	0.075244	−0.120703	0.195003
Band 2	−0.408061	−0.127495	0.645432	−0.200415	0.402229	−0.362649
Band 3	−0.425436	0.195457	0.430467	−0.066202	−0.589400	0.475227
Band 4	−0.545300	−0.112276	−0.196495	0.726971	0.170703	0.006783
Band 6	0.145060	0.001843	0.031348	−0.174912	0.009438	−0.032622
Band 7	0.085075	0.023893	0.033653	−0.094337	−0.078934	0.034434

Table 4.2: Eigenvectors of combination of two multispectral image bands PC7 to PC12

Eigenvector	7	8	9	10	11	12
Band 1	0.010943	−0.067022	0.054729	0.022465	−0.101390	−0.119553
Band 2	0.239181	0.421236	0.385568	0.340561	0.452301	0.493795
Band 3	0.503544	−0.293936	0.382458	0.439419	−0.267313	−0.136119
Band 4	0.163159	−0.252727	0.157488	0.150163	−0.238484	−0.176096
Band 6	−0.022697	0.153472	−0.099361	−0.012988	0.075207	0.022621
Band 7	−0.059953	0.671592	0.115736	0.175684	−0.071511	−0.693483
Band 1	0.483622	0.122666	−0.758458	0.270728	0.045778	−0.003001
Band 2	0.122001	−0.014319	−0.198271	0.112028	0.013191	−0.007434
Band 3	−0.032946	0.032957	0.085426	−0.072520	−0.054411	0.013952
Band 4	−0.180341	0.135932	0.063353	0.077950	−0.159874	0.084312
Band 6	−0.017667	0.357411	−0.050934	−0.005693	−0.784348	0.447594
Band 7	−0.612937	−0.175077	−0.159756	0.734595	0.007127	0.056542

for those which their coefficients for desirable bands are dominant.

In Tables 4.1 and 4.2, the first PC highlights flooded area in the second image because it is the dominant change. Also in PCs 11 and 4, the critical spectral bands in the both images are eminent. So, we select these three PCs to represent the characteristic of both images and also the change between them.

In Figure 4.12, most of the important details about the river in both images are referred. In the right part of figure, we can see that the flooded area appears green, the area covered by water in both date appears pink and the area was dry in the first date

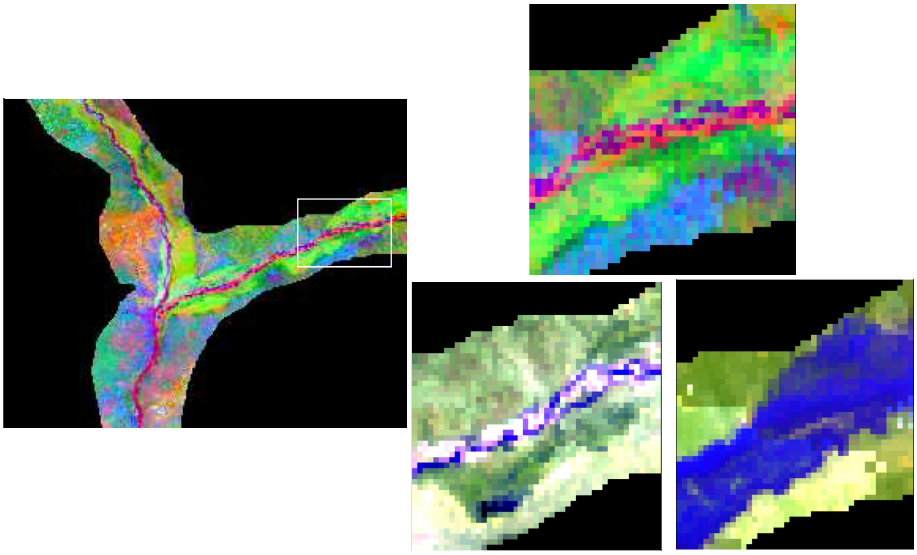

Figure 4.12: Comparison of merged data transformation and original images

and cover by water in the second date look like orange. This kind of product is useful to understand the behaviour of the object and also comparison between different data set. For interpretation, we still need the original images and this is one of the drawback of this method.

A common way to detect the change in the multitemporal images is to study the difference between them. The difference in value of same pixel in two images represent the change in physical characteristic if two images have the same radiometric basis. To detect the significant change and also eliminate the trivial in pixel values variation, we can apply PCA on image difference.

Based on Figure 4.13, difference image bands are reshaped as a two dimension matrix, then PCA is applied on the matrix and finally the transformed matrix is reshaped to its original form. We apply this technique on images represented in 4.11. To eliminate the noise of the product we must select appropriate PCs.

In the Figure 4.14, the eigenvalues of different PCs is presented. We assume that last PCs just contain noise because their eigenvalues are less than 0.001. So here first three PCs are used to reconstruct the image difference. We can conclude that there is no important information after PC3. So, we decide to reconstruct the image difference considering just first three PC.
After reconstruction the image, we can see that the quality of the image is significantly improved. In the middle image of Figure 4.15, it is easier to detect the pixels in which significant change in their value are occurred. In the last image, two thresholds are appointed into the image values for specifying the changed pixels. In the example, the constant area in both epochs appears red. Green indicate the area covered by water on

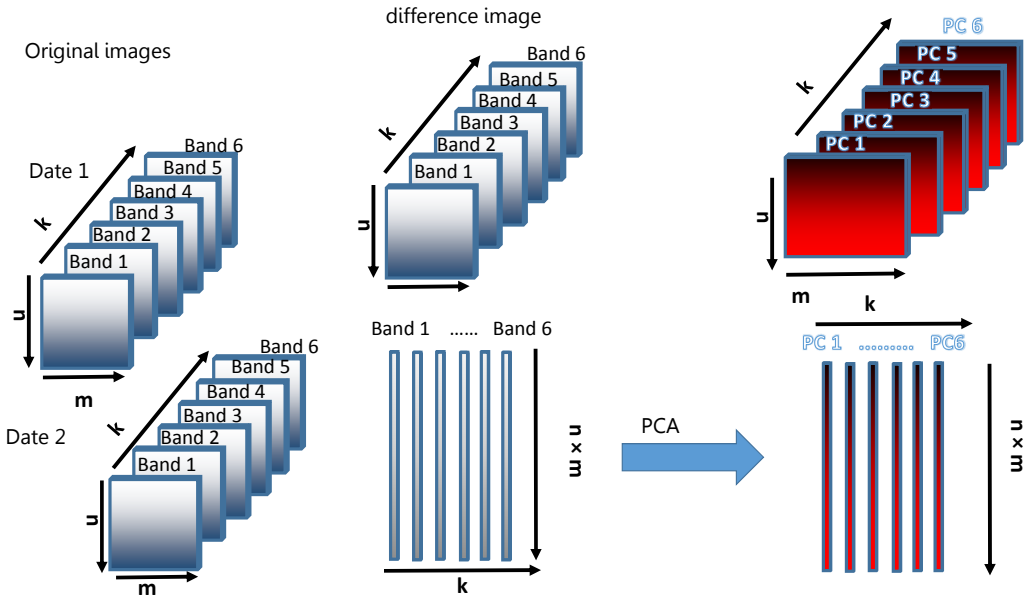

Figure 4.13: Procedure of applying PCA on a difference image

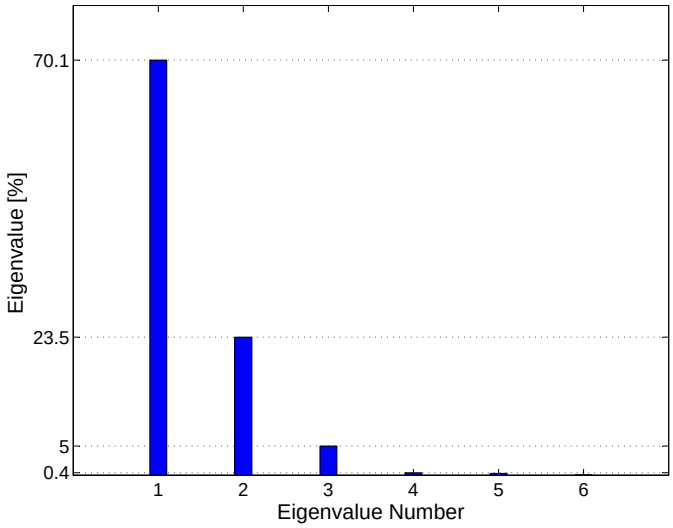

Figure 4.14: Eigenvalue of correlation matrix of image difference

the first and dry on the second epoch. Finally, the dry area on the first date changed to water on the second date is shown blue.

In the last example, the PCA is applied to bunch of images from the same area at different dates. All the images of a section of Niger river in a certain time frame are collected. After that for each image, NDVI product are generated based on equation (4.1). NDVI is a numerical indicator to assess about the density of vegetation in the

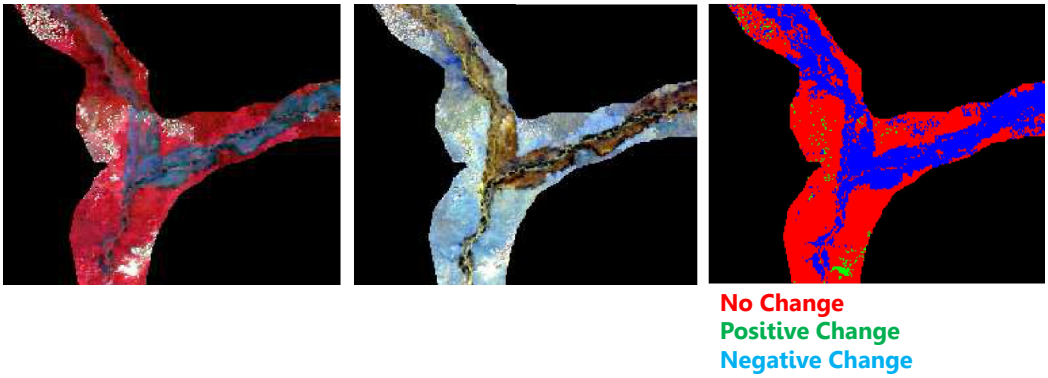

Figure 4.15: (Left) image difference, (middle) reconstruction of image difference with just first three PCs, (right) classification of the enhanced image

area. This product also can be applied to detect the surface water while very low values are specified for water. Then to define the water area, all of them are classified separately applying a threshold on NDVI image histogram.

$$\mathrm{NDVI} = \frac{(\mathrm{NDVI} - \mathrm{Red})}{(\mathrm{NDVI} + \mathrm{Red})} \tag{4.1}$$

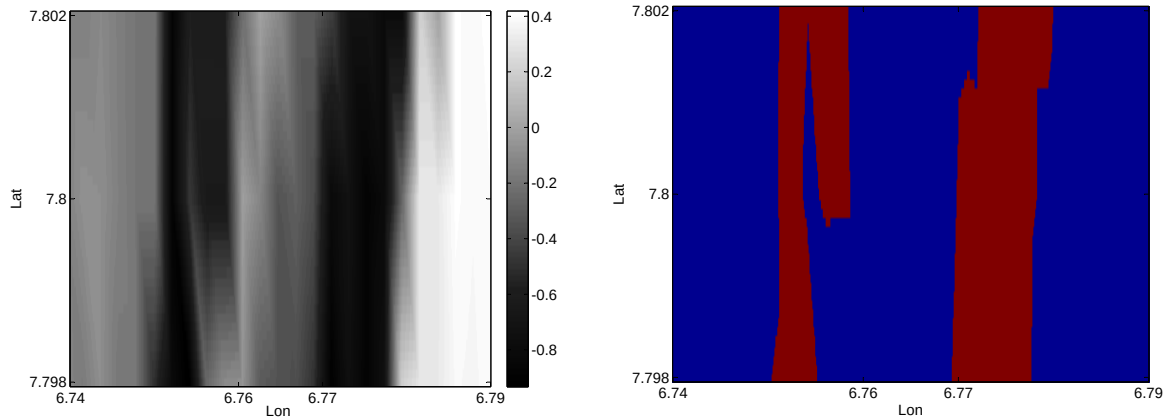

Figure 4.16: (Left) NDVI product of Niger River , (right) determination of water extent applying a threshold on images value

Finally, to monitor the change in the river width, water area in all images in a certain time period are compared together. In Figure 4.17, the water area of the river section are plotted as a time series.

We try to reduce the noise level by applying PCA on images before classifying them separately. Each image represents the situation of the river section at certain date. So annual and seasonal change in the water area will highlight in the first PCs, then change in the vegetation as a miner change will be presented in the other PCs and at the end the

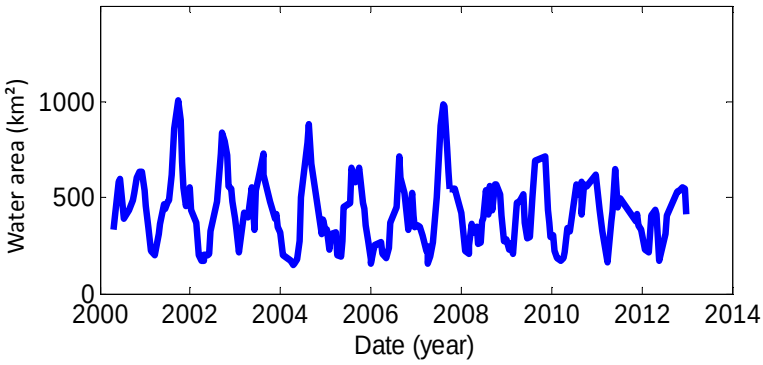

Figure 4.17: Monitoring the water area at a river section during fourteen years

noise and unimportant change will concentrate in the last PCs. Like previous studies, images are reshaped in a way that each column dedicates to the pixels of a date. PCA is applied to the new two dimensional matrix. At the end, the appropriate number of PCs to reconstruct the images is define by looking at their eigenvalues.

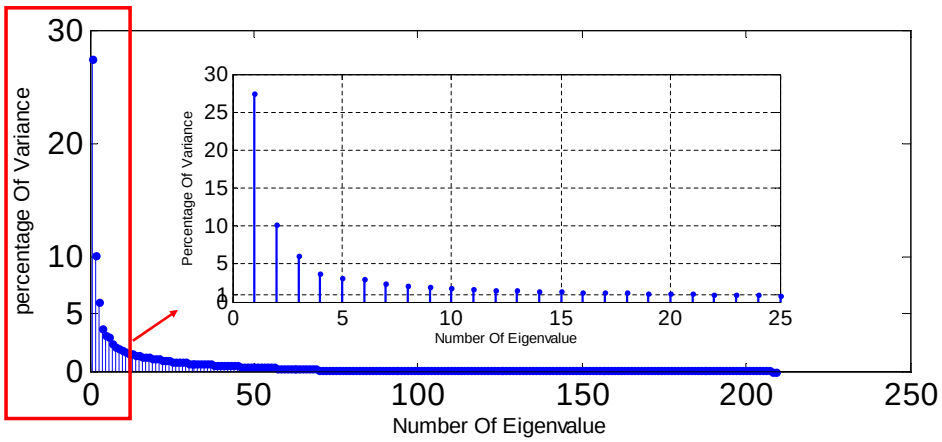

Figure 4.18: Eigenvalues of the images

In Figure 4.18, we see that the major part of the variance concentrates in the first ten PCs (more than 60%). Also it is clear that after 21th PC, each PC carries less than 1% and we can surly say that there is no information after 50th PC because they have approximately no contribution in the variance. In this example, we assume that there is no valuable information in PCs contained less than 1% of the total variance. So, we reconstruct all the images with just the first 21 PCs and generate water mask for each epoch and finally measure the water area in the appoint section.

Comparing two time series indicate that the modified one mostly follows the original time series. But in some dates, especially while the area is minimum and maximum,

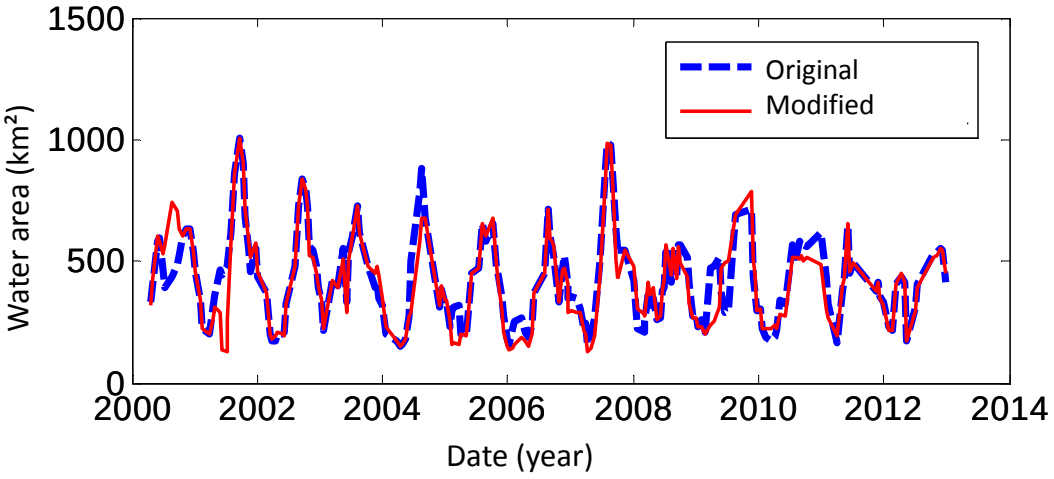

Figure 4.19: Comparison between normal and modified water area

we see the difference between two time series. When the water area is so small, it reached to the limitation based on the spatial resolution of images for each pixel). So it is possible to modify by PCA. The variation of water area is so much in the wet season, so they are also subject to modify by PCA.

In this chapter, the potential of MAD and MAF transformations for change detection application are evaluated specially in hydrological applications while water is clearly distinguishable from dry land. Also, PCA is applied mainly to reduce the noise level and also highlight the change

Chapter 5

Conclusions and outlook

Detecting water content in a remote sensing satellite images over time become a common way to monitor spatial change in inland water bodies. Water always appears very dark in near infrared and infrared bands, so most of the developed methods to detect the water in the image are based on finding a threshold for image values histogram to classify the image into two class water or land. Making the decision making the decision about pixels whether they are water or land is not always an straightforward procedure everywhere because of complicated relationship between wet and dry lands spatially in the coastal zones and shallow water. Multispectral transformations establish a linear relationship between different image bands to generate a set of new components. Unlike ordinary multispectral satellite images, transformed product bands are ordered in respect to their contribution in the covariance (correlation) between all original bands. It means that valuable information from all spectral bands congregates in the first components, so the last components contain noise.

In this thesis, different multispectral transformations on different images are applied. Our aim is to evaluate how these transformation can enhance the quality of images and reduce the noise level. Also, apply them to multitemporal images to assess their performance in change detention.

In section three, we apply PCA to each image separately to isolate the noise in the last PCs and compile valuable information in all spectral bands in the first PCs. To select the appropriate PCs, two approaches were followed. First, the PCs containing the majority of total correlation are selected to reconstruct the images. The result (Figure 3.6) showed that if only a number of primary PCs are selected and the rest is ignored, the final output is a clear image which is easier to detect the borderline of the river. In the next experiment, to select appropriate PCs for reconstructing the image, we rely on physical interpretation of different spectral bands. For example, in our study we want to highlight the information about the water content. So first we define which spectral band provides most valuable information about water content and then we choose the PCs in which the selected spectral bands have bigger coefficient. Figures 3.8 and 3.9 indicated that if the PCs are carefully selected based on the research goal, the reconstructed image or even the PCs themselves can exhibit better the image

specifications.

In section four, multitemporal images are considered as a single matrix to which apply transformations. First CCA was applied on two different Landsat 8 images to derive MAD variations. MAD has special characteristics make it valuable tool in change detection for example it is invariant to gain and offset between image bands. To define the change between two images like PCA, primary elements are considered. For example in Figure fig:sfig416 different type of change in river boundaries, vegetations and cloud coverage pattern are highlighted and presented with different color. In the next step to improve the quality of the the final product and then to magnify the area with high correlation change MAF transformation apply to MAD variations . Figure 4.9 showed that this transformation is a promising techniques because in the final result most of the major change between two images were captured also there is no need for radiometric normalization between images. Like PCA, interpreting the products of these transformations are not possible if the original images are not considered.

In the second part of fourth chapter PCA was applied on two images simultaneously. The result was a number of PCs which is equal to sum of the two images bands. If the PCs are selected carefully, the resulting image illustrates the state of the river in both epochs and also the change that occurred in between. Assigning each color to a physical attribute is the biggest obstacle in these techniques. At the end again the power of PCA to isolate noise was shown in two different examples. First (Figure 4.15) PCA was applied to an image difference to highlight the change in the first PCs and then by applying two thresholds the change area were highlighted. Finally it was applied to a time series of data to reduce the noise level (Figure 4.19). In this approach, the main concern is finding the optimum number of PC for recuperating in a way that without loosing any information, most of the noise component are removed.

Different examples of multispectral transformation applications in water area change detection in this study prove that they can be applied as tool to change the order of image bands in a way that most of the valuable information concentrate in the first elements and also noise component isolates in the last elements. However, their efficiency are highly decreased if the original images partially covered by clouds. In Figure 4.8 and4.6 we can see how clouds in both images impose themselves as biggest change in the final result and also diminishes the evident change between two images. Moreover, interpenetration of change is usually ambiguous and in most cases applying a threshold is needed. Comparing with the original images is the most reliable way to interpret the change.

Multispectral transformations have the potential to use in change detection studies for hydrological applications because the change between water and land is dominant in most spectral bands and also in the first components of transformed images. Finding a way to decrease the effect of change in other parameters like vegetation could be the

next step of this study. Applying MAD/MAF transformation to a number of multitemporal images to derive change maps and generate the time series of water area is also an outlook of this study. Also, monitoring the change in the water extent applying KT transformation provides the opportunity to convert satellite images from different sensors into a same numerical base. In this way, water area time series derived from wetness component of this transformation is the next step of this research.

Bibliography

Adams, J. B., D. E. Sabol, V. Kapos, R. A. Filho, D. A. Roberts, M. O. Smith, and A. R. Gillespie, Classification of Multispectral Images Based on Fractions of Endmembers : Application to Land-Cover Change in the Brazilian Amazon, *4257*(94), 1993.

Alsdorf, D. E., and D. P. Lettenmaier, Tracking fresh water from space., *Science (New York, N.Y.)*, *301*(5639), 1491–4, doi:10.1126/science.1089802, 2003.

Alsdorf, D. E., E. Rodriguez, and D. P. Lettenmaier, MEASURING SURFACE WATER FROM SPACE, (2006), 1–24, doi:8755-1029/2006RG000197, 2007.

Baker, K., Singular value decomposition tutorial, *The Ohio State University*, 2005.

Bazi, Y., L. Bruzzone, and F. Melgani, Image thresholding based on the EM algorithm and the generalized Gaussian distribution, *Pattern Recognition*, *40*(2), 619–634, 2007.

Birkett, C., L. Mertes, T. Dunne, M. Costa, and M. Jasinski, Surface water dynamics in the amazon basin: Application of satellite radar altimetry, *Journal of Geophysical Research: Atmospheres (1984–2012)*, *107*(D20), LBA–26, doi:10.1029/2001JD000609, 2002.

Borga, M., Learning Multidimensional Signal Processing, Ph.D. thesis, Linköping University, 1998.

Brivio, P. A., R. Colombo, M. Maggi, and R. Tomasoni, Integration of remote sensing data and GIS for accurate mapping of flooded areas, *International Journal of Remote Sensing*, *23*(3), 429–441, 2002.

Bustos, C., O. Campanella, K. Kpalma, F. Magnago, and J. Ronsin, A method for change detection with multi-temporal satellite images based on principal component analysis, in *Analysis of Multi-temporal Remote Sensing Images (Multi-Temp), 2011 6th International Workshop on the*, pp. 197–200, IEEE, 2011.

Canty, M. J., and A. a. Nielsen, Automatic radiometric normalization of multitemporal satellite imagery with the iteratively re-weighted MAD transformation, *Remote Sensing of Environment*, *112*(3), 1025–1036, doi:10.1016/j.rse.2007.07.013, 2008.

Canty, M. J., A. A. Nielsen, and M. Schmidt, Automatic radiometric normalization of multitemporal satellite imagery, *Remote Sensing of Environment*, *91*(3), 441–451, 2004.

Cao, W., Change detection using SAR data, Master's thesis, university of Stuttgart, 2013.

Coombe, G., An introduction to principal component analysis and online singular value decomposition, *graduate paper, University of North Carolina, Chapel Hill, NC*, 2006.

Crétaux, J.-F., and C. Birkett, Lake studies from satellite radar altimetry, *Comptes Rendus Geoscience*, *338*(14-15), 1098–1112, doi:10.1016/j.crte.2006.08.002, 2006.

Crist, E. P., and R. C. Cicone, A Physically-Based Transformation of Thematic Mapper Data—The TM Tasseled Cap, *IEEE Transactions on Geoscience and Remote Sensing*, *GE-22*(3), 256–263, 1984.

Du, Y., P. M. Teillet, and J. Cihlar, Radiometric normalization of multitemporal high-resolution satellite images with quality control for land cover change detection, *Remote Sensing of Environment*, *82*(1), 123–134, 2002.

Eklundh, L., and A. Singh, A comparative analysis of standardised and unstandardised principal components analysis in remote sensing, *International Journal of Remote Sensing*, *14*(7), 1359–1370, 1993.

Fung, T., and E. Ledrew, Application of principal components analysis to change detection, *Photogrammetric engineering and remote sensing*, *53*(12), 1649–1658, 1987.

Gao, H., C. Birkett, and D. P. Lettenmaier, Global monitoring of large reservoir storage from satellite remote sensing, *Water Resources Research*, *48*(9), 2012.

Gong, P., Change detection using principal component analysis and fuzzy set theory.pdf, 1993.

Hotelling, H., Relations between two sets of variates, 1936.

Joyce, K. E., S. E. Belliss, S. V. Samsonov, S. J. McNeill, and P. J. Glassey, A review of the status of satellite remote sensing and image processing techniques for mapping natural hazards and disasters, *Progress in Physical Geography*, *33*(2), 183–207, 2009.

Kauth, R. J., and G. S. Thomas, The tasselled cap a graphic description of the spectral temporal development of agricultural crops as seen by Landsat, in *LARS Symposia*, p. 159, 1976.

Klein, I., A. J. Dietz, U. Gessner, A. Galayeva, A. Myrzakhmetov, and C. Kuenzer, Evaluation of seasonal water body extents in Central Asia over the past 27 years derived from medium-resolution remote sensing data, *International Journal of Applied Earth Observation and Geoinformation*, *26*, 335–349, doi:10.1016/j.jag.2013.08.004, 2014.

Li, C. H., and C. K. Lee, Minimum cross entropy thresholding, *Pattern Recognition*, *26*(4), 617–625, 1993.

Lu, D., P. Mausel, E. Brondizio, and E. Moran, Change detection techniques, *International journal of remote sensing*, *25*(12), 2365–2401,

doi:10.1080/0143116031000139863, 2004.

Martinis, S., A. Twele, and S. Voigt, Towards operational near real-time flood detection using a split-based automatic thresholding procedure on high resolution TerraSAR-X data., *Natural Hazards & Earth System Sciences*, *9*(2), 2009.

Martinis, S., A. Twele, C. Strobl, J. Kersten, and E. Stein, A Multi-Scale Flood Monitoring System Based on Fully Automatic MODIS and TerraSAR-X Processing Chains, *Remote Sensing*, *5*(11), 5598–5619, 2013.

McGinley, M., Niger river, 2013.

Munyati, C., Use of principal component analysis (PCA) of remote sensing images in wetland change detection on the Kafue Flats, Zambia, *Geocarto International*, *19*(3), 11–22, 2004.

Nielsen, A. A., Analysis of Regularly and Irregularly Sampled Spatial , Multivariate , and Multi-temporal Data by, Ph.D. thesis, Technical University of Denmark, 1995.

Nielsen, A. A., The regularized iteratively reweighted MAD method for change detection in multi- and hyperspectral data., *IEEE transactions on image processing : a publication of the IEEE Signal Processing Society*, *16*(2), 463–78, 2007a.

Nielsen, A. A., The regularized iteratively reweighted MAD method for change detection in multi-and hyperspectral data, *Image Processing, IEEE Transactions on*, *16*(2), 463–478, 2007b.

Nielsen, A. A., Kernel maximum autocorrelation factor and minimum noise fraction transformations, *Image Processing, IEEE Transactions on*, *20*(3), 612–624, 2011.

Nielsen, A. A., K. Conradsen, and J. J. Simpson, Multivariate alteration detection (MAD) and MAF postprocessing in multispectral, bitemporal image data: New approaches to change detection studies, *Remote Sensing of Environment*, *64*(1), 1–19, 1998.

Nielsen, A. A., K. Conradsen, and O. B. Andersen, A change oriented extension of EOF analysis applied to the 1996–1997 AVHRR sea surface temperature data, *Physics and Chemistry of the Earth, Parts A/B/C*, *27*(32), 1379–1386, 2002.

Papa, F., C. Prigent, F. Durand, and W. B. Rossow, Wetland dynamics using a suite of satellite observations: A case study of application and evaluation for the Indian Subcontinent, *Geophysical Research Letters*, *33*(8), 2006.

Papa, F., C. Prigent, and W. B. Rossow, Monitoring Flood and Discharge Variations in the Large Siberian Rivers From a Multi-Satellite Technique, *Surveys in Geophysics*, *29*(4-5), 297–317, doi:10.1007/s10712-008-9036-0, 2008.

Prigent, C., F. Papa, F. Aires, W. B. Rossow, and E. Matthews, Global inundation dynamics inferred from multiple satellite observations,1993–2000, *Journal of Geophysical Research: Atmospheres (1984–2012)*, *112*(D12), 2007.

Radke, R. J., S. Andra, O. Al-Kofahi, and B. Roysam, Image change detection algorithms: a systematic survey, *Image Processing, IEEE Transactions on*, *14*(3), 294–307, 2005.

Rice, J., *Mathematical statistics and data analysis*, Cengage Learning, 2006.

Richards, J. A., and X. Jia, *Remote sensing digital image analysis*, vol. 3, Springer, 1999.

Romeiser, R., H. Runge, S. Suchandt, J. Sprenger, H. Weilbeer, A. Sohrmann, and D. Stammer, Current measurements in rivers by spaceborne along-track insar, *Geoscience and Remote Sensing, IEEE Transactions on*, *45*(12), 4019–4031, 2007.

Singh, A., Digital change detection techniques using remotely-sensed data, *International Journal of Remote Sensing*, (January 2014), 37–41, doi:10.1080/01431168908903939, 1989.

Smith, L. C., and T. M. Pavelsky, Remote sensing of volumetric storage changes, *1358*(June), 1353–1358, doi:10.1002/esp, 2009.

Smith, L. C., B. L. Isacks, A. L. Bloom, and A. B. Murray, Estimation of Discharge From Three Braided Rivers UsingSynthetic Aperture Radar Satellite Imagery: Potential Application to UngagedBasins, *32*(7), 2021–2034, 1996.

Sneeuw, N., C. Lorenz, B. Devaraju, M. J. Tourian, J. Riegger, H. Kunstmann, and A. Bárdossy, Estimating runoff using hydro-geodetic approaches, *Surveys in Geophysics*, *35*(6), 1333–1359, doi:10.1007/s10712-014-9300-4, 2014.

Switzer, P., and A. A. Green, Min/max autocorrelation factors for multivariate spatial imagery, *Tech. rep.*, DEPARTMNET OF STATISTICS, STANFORD UNIVERSITY, STANFORD, CALIFORNIA, 1984.

Tourian, M., O. Elmi, Q. Chen, B. Devaraju, S. Roohi, and N. Sneeuw, A spaceborne multisensor approach to monitor the desiccation of lake urmia in iran, *Remote Sensing of Environment*, *156*, 349–360, doi:10.1016/j.rse.2014.10.006, 2015.

Tourian, M. J., N. Sneeuw, and A. Bárdossy, A quantile function approach to discharge estimation from satellite altimetry (ENVISAT), *Water Resources Research*, *49*(7), 4174–4186, doi:10.1002/wrcr.20348, 2013.

Townsend, P. A., Mapping seasonal flooding in forested wetlands using multitemporal Radarsat SAR, *Photogrammetric Engineering and Remote Sensing*, *67*(7), 857–864, 2001.

Wang, Y., Seasonal change in the extent of inundation on floodplains detected by JERS-1 Synthetic Aperture Radar data, *International Journal of Remote Sensing*, *25*(13), 2497–2508, doi:10.1080/01431160310001619562, 2004.